rck 4/21/59

Clutte

NACA TN 3101

NATIONAL ADVISORY COMMITTEE FOR AERONAUTICS

TECHNICAL NOTE 3101

STUDY OF THREE-DIMENSIONAL INTERNAL FLOW DISTRIBUTION BASED ON MEASUREMENTS IN A 48-INCH RADIAL-INLET CENTRIFUGAL IMPELLER

By Joseph T. Hamrick, John Mizisin, and Donald J. Michel

Lewis Flight Propulsion Laboratory
Cleveland, Ohio

Washington
February 1954

AQ M00-10-3207

NATIONAL ADVISORY COMMITTEE FOR AERONAUTICS

TECHNICAL NOTE 3101

STUDY OF THREE-DIMENSIONAL INTERNAL FLOW DISTRIBUTION BASED ON MEASUREMENTS IN A 48-INCH RADIAL-INLET CENTRIFUGAL IMPELLER

By Joseph T. Hamrick, John Mizisin, and Donald J. Michel

SUMMARY

The flow distribution throughout the passage of a rotating impeller has been studied in detail, and the results are presented in the form of relative velocity and relative pressure loss contours. These were computed from total-pressure measurements taken at numerous positions from blade to blade and hub to shroud and from static pressures measured on the impeller hub.

The loss and velocity distributions indicate that secondary flows in the boundary layer tend to shift the low-energy air toward the blade suction surface within the passage. There is a counter effect at the shroud apparently caused by leakage through the blade-to-shroud clearance space which moves the low-energy air toward the pressure surface. This results in a concentration of low-energy air at approximately 80 percent of the passage width from the pressure face at the shroud.

Comparison of the data from the internal measurements made for the impeller of this investigation with hot-wire anemometer studies made at the outlet of a similar impeller indicates that much can be learned about the internal flow picture with hot-wire surveys alone.

INTRODUCTION

A number of solutions for isentropic compressible flow through radial and mixed flow impellers have been made (refs. 1 to 4, for example). These solutions and the methods by which they were obtained were presented in an effort to create a better general understanding of the flow conditions in centrifugal compressors and to provide guidance in impeller design. In the use of these analysis methods as well as of design methods such as that of reference 5, departure from the isentropic case is expected with the introduction of a viscous fluid. In order to utilize these design and analysis methods most effectively, some knowledge of the manner in which viscosity affects the over-all flow distribution is desirable. Some viscosity effects may be explored theoretically, as in the secondary flow studies of reference 6, but for the most part, actual flow measurements are necessary.

Experimental investigations of the flow conditions at mean blade height within the rotating passages of a 48-inch radial-inlet centrifugal impeller operating at low tip speed have been made and reported in references 7 through 10. These investigations showed that toward the passage exit large losses in relative total pressure had occurred near the trailing (suction) surface of the blade, whereas the flow near the driving (pressure) surface suffered little or no loss in relative total pressure. This distribution probably resulted, for the most part, from secondary flow movements such as those discussed in references 6 and 11. Studies of the flow at the impeller exit by means of a hot-wire anemometer (ref. 12) showed that the variation in velocity, and therefore the relative total-pressure loss, from blade to blade varied greatly from hub to shroud. However, it was difficult to determine from the anemometer studies alone the exact cause of the observed distribution.

In order to obtain a better analysis of the flow distribution throughout the rotating impeller passage, total-pressure measurements were taken at several locations between the hub and shroud as well as from blade to blade on a 48-inch-diameter radial-inlet impeller similar to that of references 7 to 10 but of different blade shape. This investigation was made at the NACA Lewis laboratory, and the experimental results are presented in the form of relative velocity and relative total-pressure-loss contours.

APPARATUS, INSTRUMENTATION, AND PROCEDURE

Test rig. - The test rig and rig instrumentation, excluding the impeller, are identical to that given in reference 7 with the following addition: The over-all total pressure and temperature were measured in the diffuser at the $1\frac{1}{2}$ impeller radius position near the vaneless diffuser outlet in three peripheral locations. Four-probe rakes were used at each location for both temperature and pressure. A cutaway view of the compressor rig is shown in figure 1.

The impeller blade shape is different from the blade shape of the impeller used in references 7 to 10 in that the shape used in this investigation produces a more abrupt loading and unloading of the blade near the inlet and exit, respectively. The clearance between the impeller and the stationary front shroud is 0.050 inch.

Impeller instrumentation. - Pressure measurements were made at the encircled positions in the impeller passage shown in figure 2. The lines from inlet to outlet along which the instruments are placed at each radius are referred to for convenience as geometric streamlines. They have no relation to streamlines for potential flow. Static pressures were measured through 0.030-inch-diameter orifices in the impeller hub. Total-pressure measurements were made by means of shielded total-pressure probes at the levels shown on the impeller photograph in figure 3. A calibration of the probe showed a negligible error for a flow angle range of $\pm 40^{\circ}$. The probes were pointed in a direction parallel to the geometric streamlines shown in figure 2 and were distributed among the 18 passages to prevent uneven blockage as much as possible. The total-pressure probe locations are also shown by the encircled positions on a typical cross section in figure 4.

The total-pressure probe (fig. 5) was so fabricated that it could be reduced in height successively from level 0 to level 5 by unsoldering the joint nearest the hub, reducing the length of the telescoping parts, and resoldering. The removal or installation of the probes was made on the blade side of the hub at the point of rig disassembly shown in figure 3.

Pressure-transfer device. - The pressure-transfer device, a section of which is shown in figure 6, is the same as that used in reference 7 with the following important alteration: In the original assembly the outer spacer (fig. 6) as well as the rotating inner spacer had annular projections for spacing the bearings. Positioning of the bearing from both the inner and outer race resulted in end thrust upon the bearings which caused failure. The trouble was eliminated by removing the annular projections in the outer spacers which, as a result, now serve only to make up the outer jacket.

Procedure. - The compressor was operated at a corrected tip speed $U/\sqrt{\theta}$ of 700 feet per second over a range of corrected air weight flows $W\sqrt{\theta}/\delta$ from choking to incipient surge. (All symbols are defined in the appendix.) All runs were made at ambient inlet air temperatures (70° to 90° F) and an inlet air stagnation pressure of approximately 16 inches of mercury. The procedure used in making pressure measurements on the rotating impeller and the required corrections are the same as those given in reference 7. Theoretical pressures were computed by the method of reference 2, and experimental velocities were computed by the equations given in reference 9.

ACCURACY OF RESULTS

For each weight flow at each level, it was necessary to reposition the pressure-transfer device five times. As a result, to obtain complete data for all blade heights at one weight flow, 30 repeat runs were required. It was therefore necessary to control closely the weight flow and impeller speed. In setting the weight flow $W\sqrt{\theta}/\delta$, the maximum deviation from the average was 1.0 percent and generally less than 0.5 percent. The maximum deviation from average in setting the tip speed $U/\sqrt{\theta}$ was 0.3 percent. The smoothness with which the plotted points fall in line for the many runs indicates that adequate control was maintained.

Screening of the data was accomplished in two steps. The first step consisted of checking any manometer readings which appeared out of line during rig operation by testing for leaks in the lines leading from the impeller to the manometer boards after completion of a run. These leaks were usually a result of failure of the seals in the transfer device. The second step consisted of a continuity check in which the static and total pressures were plotted against distance in two directions in the blade-to-blade plane and the total pressure only was plotted against probe height.

Points that appeared to be out of line were checked with the data on leaks recorded in the first step. If a leak had occurred and the shape of the curve could not be determined without the point, a rerun of the point was made. Reruns for points near the driving face in the latter half of the passage were not considered necessary inasmuch as values in that region had been found to be very close to the theoretical value (refs. 7 to 10). Some effects are introduced by interference from the total-pressure probes and approximations required in regard to static pressure; however, comparisons of the data with theoretical values indicate that the results are reliable.

Total pressure. - Inasmuch as little or no losses in relative total pressure are experienced on the blade driving face for positive angles of attack, the total pressures nearest the pressure face (stream surface 1) have been compared with the theoretical values in figure 7. The angle of attack is defined as the angle between the average flow direction of the air at the inlet and the blade driving face; flow directed at the driving face forms a positive angle of attack. The weight flow of 29.3 pounds per second was chosen because it gives a positive angle of attack and is near maximum efficiency. Except near the shroud at the 13 and 14 inch radii, the theoretical and experimental values agree very well. The reliability of the total-pressure probes based upon this agreement is very good. The points not shown are those for which leaks occurred.

Probe interference. - The effect of probe interference can be shown by changes in over-all efficiency with change in probe height. At the maximum weight flow in figure 8 there is an increase of 18 points in adiabatic efficiency in going from level 0 (maximum probe height) to level 5. For the weight flow of 29.3 pounds per second, the effect is of the order of only 1 point in efficiency. For the lower weight flows (not shown), it is less.

Static pressure. - Static pressures were measured at the hub only at points corresponding to the bases of the total-pressure probes. The data of reference 7 show that there is very little variation in static pressure from hub to shroud across the blade surface at a given radius for this hub-shroud configuration and that the static pressure measured on the shroud is very close to the average across the impeller passage from blade to blade at a given radius. In figure 9 the average shroud static pressure for all levels of the total-pressure probes is compared with the corresponding average static pressures on the hub. This average is typical for the individual runs for each level. There is some difference at the 13, 14, and 16 inch radii; however, no attempt was made to allow for this variation from hub to shroud in computing velocities for the various levels at these radii, inasmuch as this variation as well as the deviations from the average are such that the over-all velocity configuration is not significantly affected. In figure 10 the average static pressure for all levels near the driving and trailing faces is compared with the theoretical value as computed by the method of reference 2. Although the magnitudes do not agree because of boundary layer displacement and viscous losses in the experimental case, the curves have similar shapes.

RESULTS AND DISCUSSION

Over-All Performance

The average over-all performance for all levels of instrumentation within the passage is shown in figure 11(a). Below 29.3 pounds per second the efficiency for each level is within approximately 1 percent of the average value for all levels. For weight flows of 29.3 pounds per second or above, the efficiency for each level is given in figure 8. In figure 11(b) the average relative adiabatic efficiency at the 23.5-inch radius (0.5 in. from the impeller exit) is shown for comparison with the over-all adiabatic efficiency. The two curves are approximately parallel except at the minimum or surge weight flow, which is discussed subsequently. The difference at each weight flow between the relative and over-all efficiency may be indicative of the mixing losses which take place between the two measuring points. Relative adiabatic efficiency $\eta_{ad,rel}$ is defined (ref. 7) as

$$\eta_{ad,rel}=\frac{\Delta H_{ad}}{\Delta H_{act}} \qquad (1)$$

where from the inlet to a given radius, ΔH_{ad} is the isentropic enthalpy rise relative to the impeller which will give the measured relative total pressure, and ΔH_{act} is the actual increase in relative enthalpy (based on impeller speed).

If it is assumed that there are no losses between the impeller exit and the over-all measuring station, then in the absence of inlet prewhirl

$$\Delta H_{ad} = \Delta H_{act} - \frac{f_s U^2}{gJ}(1 - \eta_{ad}) \tag{2}$$

where f_s is the slip factor.

At the impeller exit (ref. 7),

$$\Delta H_{act} = \frac{U^2}{2gJ} \tag{3}$$

Combining (1), (2), and (3) gives

$$\eta_{ad} = 1 - \frac{1 - \eta_{ad,rel}}{2f_s} \tag{4}$$

The slip factor at a weight flow of 29.3 pounds is 0.85 with an average relative adiabatic efficiency of 0.91 at the 23.5-inch radius. With no losses downstream of this point, the over-all adiabatic efficiency would be 0.95 as compared with the actual value of 0.81. This indicates large mixing losses.

Performance within the Passage

Presentation of results. - The static- and total-pressure measurements within the passage were used to determine the internal relative velocity distribution. In addition, the pressure loss distribution was obtained by subtracting the measured relative total pressure from the theoretical relative total pressure computed on the basis of impeller speed. These are presented in the form of contour plots as ratios of inlet stagnation velocity of sound and inlet stagnation pressure, respectively, in figures 12 to 19 for weight flows from 11.2 to 45.1 pounds per second. Pressure-loss-ratio contours for passage cross-sectional views are presented to show the loss configuration from hub to shroud. Figure 19 shows all passage cross-sectional views in one figure for a more convenient comparison of losses with varying weight flow. The curves of figure 20 may be used to determine the relative adiabatic efficiency for any given pressure loss.

General observations. - Except for the weight flows of 11.2 and 45.1 pounds per second, the pressure loss ratio near the driving face is of the order of 0.01 or less. This agrees with the data of references 7 to 10, which tend to substantiate the fact that, except for extreme off-design conditions, low-energy particles do not remain on or near the blade driving face. In at least one radial position for each weight flow there is a high loss region near the shroud at approximately 80 percent of the passage width from the driving face.

Surge weight flow. - There is a gradual shift in the flow configuration with increasing weight flow, and the general pattern is maintained except at the surge weight flow of 11.2 pounds. One deviation from the general pattern is in the pressure loss ratio in the vicinity of the driving face (fig. 12(b)) where the loss is as great as or greater than that for any other weight flow except for 45.1 pounds per second, where such losses would be expected to result from the high negative angle of attack. These losses are probably due to back flows such as those discussed in reference 13. Flow reversals in the passage cause air particles, to which rotation has been imparted, to flow back into the air stream ahead of the inlet. These particles lose part or all of their rotational energy and reenter the passage at a higher temperature, thereby constituting a low-energy air mass.

A second deviation is in the larger difference, at this weight flow, between the relative and over-all adiabatic efficiency (fig. 11(b)) even though the velocity configuration (fig. 12(a)) appears good and the measured pressure loss is not excessive. A possible explanation is as follows: If the component of the relative velocity associated with the volume flow rate through the impeller passage is not large enough to effectively cancel the eddy motion which is caused by the absolute irrotationality of the fluid particles, then a portion of the eddy remains and is attached to the driving face of the blades as shown in the flow solutions of reference 1. The reverse flow on the driving face for the flow solutions at low weight flow in reference 9 also indicates the presence of the eddy; however, in this investigation, as well as those of references 7 to 10, there has been no direct experimental evidence of the eddy, which may be explained by flow instability. If the eddy occurred, it is likely that it was unstable and occurred in only a few of the passages at a given instant, rotating about the impeller somewhat in the manner described for rotating stall in reference 14. The total-pressure probes in this case would give a time average of the total pressure, thereby making identification of the eddy impossible. In areas of momentary reversals of flow the time average of the total pressure is meaningless. The higher-than-average pressures indicated under such conditions would account for the large difference between the relative and over-all average efficiencies obtained for surge weight flow.

Angle of attack effect. - For weight flows above surge the main variations in the flow configuration appear to be caused by variations in angle of attack. In figure 13 the effect of a high positive angle of attack is seen in the flow deceleration along the trailing face near the inlet. This deceleration leads to a rapidly thickened boundary layer and probable separation with consequent high-loss regions along the trailing face (fig. 13(b)). The cross-sectional views in figure 13(c) show a smaller loss at the hub than at the shroud for the 13- and 14-inch radii, which may be due to a smoother transition of the flow from the rotating hub into the passage than from the stationary shroud. The large loss in total pressure in the vicinity of the blade trailing face is reflected in a generally lower velocity along the trailing face than on the driving face at the weight flow of 15.6 pounds per second, a situation which exists for no other weight flow. However, this does not affect the blade loading, which in general is unaffected by the loss picture except as the average level of static pressure is affected by increased average velocity due to losses and boundary layer blockage. Fair agreement between computed and measured static pressure for all weight flows except maximum was obtained in reference 9. The agreement for this impeller at the maximum efficiency point can be seen in figure 10.

3083

The losses due to angle of attack appear to decrease with increasing weight flow (figs. 13 to 17) until the weight flow of 45.1 pounds per second is reached, where a severe negative angle of attack results in deceleration and probable separation on the driving face (fig. 18).

Secondary Flow and Clearance Effects

High loss region at shroud. - The absence of low-energy particles on the driving face and the appearance of the high-loss region at the shroud approximately 80 percent of the passage width from the driving face give rise to speculation as to what forces have acted to bring about such a distribution. Some information may be obtained by considering the pressure gradients which arise from the movement of a particle through a rotating passage.

Pressure gradient. - The equation relating the pressure gradient to the passage geometry, particle velocity, and angular velocity is obtained as follows, with all derivatives with respect to time being substantial derivatives:

From reference 15,

$$\frac{1}{\rho}\frac{\partial p}{\partial r} = \frac{u^2}{r} + r\omega^2 + 2\omega u - \frac{dv}{dt} \tag{5}$$

$$\frac{1}{\rho r}\frac{\partial p}{\partial \theta} = -\frac{du}{dt} - \frac{uv}{r} - 2v\omega - \frac{d\omega}{dt} \tag{6}$$

(Orientation of quantities used is given in fig. 21.)

$$u = q \sin \beta \qquad v = q \cos \beta \qquad \frac{d\omega}{dt} = 0$$

Differentiating with respect to time gives

$$\frac{du}{dt} = \sin \beta \frac{dq}{dt} + q \cos \beta \frac{d\beta}{dt}$$

$$\frac{dv}{dt} = -q \sin \beta \frac{d\beta}{dt} + \cos \beta \frac{dq}{dt}$$

From figure 21,

$$q\ dt = (d\beta + d\theta')\ r_c$$

$$q \sin \beta\ dt = r\ d\theta'$$

Combining the two previous equations gives

$$\frac{d\beta}{dt} = \frac{q}{r_c} - \frac{q \sin \beta}{r} \tag{7}$$

Then

$$\frac{du}{dt} = \sin \beta \frac{dq}{dt} + \frac{q^2 \cos \beta}{r_c} - \frac{q^2 \sin \beta \cos \beta}{r} \tag{8}$$

$$\frac{dv}{dt} = -\frac{q^2}{r_c} \sin \beta + \frac{q^2 \sin^2 \beta}{r} + \cos \beta \frac{dq}{dt} \tag{9}$$

$$\frac{dp}{dn} = \frac{\partial p}{\partial r}\frac{dr}{dn} + \frac{\partial p}{\partial \theta'}\frac{d\theta'}{dn} = \frac{\partial p}{\partial r} \sin \beta - \frac{1}{r}\frac{\partial p}{\partial \theta'} \cos \beta \tag{10}$$

Substituting equations (5), (6), (8), and (9) in (10) gives

$$\frac{1}{\rho}\frac{dp}{dn} = \omega^2 r \sin \beta + 2\omega q + \frac{q^2}{r_c} \tag{11}$$

Thus, it can be seen that with large variations in q from hub to shroud, such as those from the 18-inch radius to the outlet shown in figure 22, there must be comparable variations in β and r_c to maintain constant dp/dn from hub to shroud across a geometric stream surface. Inasmuch as actual values of β and r_c are not known in this case, the secondary flow velocity components cannot be determined; however, a rough indication of the direction of the secondary flow can be obtained as follows: If it is assumed that the relative velocity is directed along the geometric streamlines, values of dp/dn may be computed from the actual relative velocity and values of β and r_c for the geometric streamlines. Inasmuch as the relative velocity varies from hub to shroud, the values of dp/dn thus computed will also vary, but it has been shown experimentally that there is only slight variation in the blade-to-blade pressure gradient from hub to shroud across a geometric stream surface. Therefore some average value of dp/dn would be sought by the fluid in motion and accelerative forces which move the fluid in a direction other than along the geometric stream surface would come into play.

Secondary flow. - For the weight flow of 29.3 pounds per second at the 20-inch radius, values of dp/dn were computed using the actual velocities (fig. 22) and β and r_c for the geometric streamlines. At each stream surface, the computed value at each level was subtracted from the average of the computed values for all levels at the stream surface and is shown in figure 23(a). Positive values indicate an accelerative force toward the trailing face and negative values, an accelerative force toward the driving face. The suggested directions of secondary flow shown by the values given on figure 23(a) are compatible with the directions indicated by the concentration of low-energy air at the 20-inch radius in figure 16(c). The two figures were used to find the conjectured secondary flow direction shown in figure 23(b). Along the hub and shroud the gradients are such that the low-energy air in the boundary layer is moved toward the trailing face except in areas where the movement is offset by leakage through the blade-to-shroud clearance space. It appears that air of relatively high energy pours through the clearance space, expands into the area of the trailing face, and moves the low-energy air along the shroud to meet that coming from the driving face. The amount of energy involved in these secondary flows is a matter of some debate. Probably the greatest losses come from the mixing in the diffuser of the particles of varying velocity leaving the impeller exit. With the flow of low-energy air from two different directions at the shroud in the impeller passage, there is a possibility that the low-energy air mass near the shroud at approximately 80 percent of the passage width from the driving face is in the form of a vortex. If that is the case, the mixing losses which accompany the dissipation of the vortex in the vaneless diffuser would help to explain the large discrepancy between the relative and over-all adiabatic efficiencies.

Clearance effects. - The efficiency may be improved by proper choice of clearance space, as shown by the experimental results of references 16 and 17. In each of these cases the over-all efficiency was improved by decreasing the clearance space, except near maximum flow. Near maximum flow the reduction in efficiency is probably a Mach number effect due to reduction in flow area rather than a clearance effect. It appears from the data contained herein that a reduction in clearance space would tend to move the high-loss regions on the shroud toward the trailing face. Removal of the clearance by fully shrouding the impeller may appear to be the obvious method of reducing losses; however, there is some evidence (refs. 11 and 18) that full shrouding may not be desirable, especially at higher impeller speeds. A possible explanation is as follows: The theoretical calculations of reference 1 show that as the impeller tip speed is increased for a given weight flow there is an increase in the velocity difference from driving face to trailing face, which results primarily from a decrease in velocity along the driving face except near the outlet. The resulting greater deceleration along the driving face near the impeller inlet increases the tendency toward boundary layer build-up. If in the absence of a clearance space (which apparently acts as a boundary layer bleed for the unshrouded impeller) the secondary flows in the hub and shroud boundary layer are insufficient to remove the boundary layer from the driving face, large losses due to boundary layer build-up on the driving face may result.

COMPARISON WITH HOT-WIRE ANEMOMETER SURVEYS

For the impeller of references 7 to 10, hot-wire anemometer surveys were made just downstream of the impeller outlet and are reported in reference 12. Although the impeller used in this investigation has a different blade shape, the loss patterns for the two impellers are similar. In figure 24, which was taken from reference 12, it can be seen that for low values of D, where D is percent of distance from hub to shroud, small losses exist near the blade trailing face with the losses increasing toward the shroud. At D = 0.5, which corresponds to level 3, the major loss region is still adjacent to the blade; but at D = 0.79, which corresponds to level 2, the region of maximum loss has moved farther toward midpassage; and at D = 0.96, which corresponds to level 0, the maximum losses are definitely not adjacent to the blade trailing face. The sharp fluctuations at D = 0.96 give further evidence that a vortex has formed on the shroud. The results of surveys taken radially outward from the impeller are also shown in reference 12. Evidence of the general flow pattern at the impeller outlet still exists at a radius 23 percent greater than that of the impeller. The persistence of this flow pattern also suggests the existence of a vortex.

In view of the fair agreement shown between the internal measurements and the hot-wire anemometer surveys even for impellers of different blade shape, it appears that a great deal can be learned about the internal flow picture with hot-wire surveys alone.

SUMMARY OF RESULTS

A detailed study of the flow distribution throughout the passage of a rotating impeller has been made, and the flow distribution is presented in the form of relative velocity and relative pressure loss contours. These were computed from total-pressure measurements taken at numerous positions from blade to blade and hub to shroud and from static pressures measured on the impeller hub. The following observations are made:

1. Except at large negative angles of attack, the driving face (pressure surface) of the blade and the adjacent area are relatively free of low-energy air, which agrees with previous experimental results.

2. There is a small concentration of very-low-energy air on the trailing face (suction surface) of the blade immediately adjacent to the hub.

3. There is a roll-up of low-energy air, which may be in the form of a vortex, on the shroud approximately 80 percent of the passage width from the driving face.

4. There are large variations in the hub-to-shroud velocity profiles from the 18-inch radius to the outlet.

5. The area of greatest over-all relative total-pressure loss is in the vicinity of the trailing face.

6. The average relative adiabatic efficiency within the passage near the impeller exit is approximately 10 points higher than the over-all adiabatic efficiency measured in the diffuser at a diameter $1\frac{1}{2}$ times that of the impeller. Large mixing losses are indicated inasmuch as the relative efficiency would have been 4 points lower than the over-all efficiency if there had been no losses in the diffuser.

7. Comparison of the data from the internal measurements made for the impeller of this investigation with hot-wire anemometer studies made at the outlet of a similar impeller indicates that much can be learned about the internal flow picture with hot-wire surveys alone.

CONCLUDING REMARKS

3083

An attempt has been made in the presentation of the results of this investigation both to provide the designer with a better insight into the effects of viscosity on the internal flow pattern and to give background information which in the future will help in the interpretation of survey data obtained at the impeller exit. It is probable that the viscous effects and the manner in which they affect the flow configuration as found in this impeller are typical qualitatively for centrifugal impellers in general. However, the relative magnitudes of the loss concentrations and their precise locations will vary with the geometric configuration. For example, it is expected that a concentration of low-energy air will be found on the shroud, but that the size and location with respect to the blades will vary with such factors as the shape of the boundary layer profile, the blade-height to passage-width ratio, and the size of the blade-to-shroud clearance space. The over-all effect of these factors upon flow distribution may be determined to an important extent by hot-wire anemometer surveys.

Lewis Flight Propulsion Laboratory
National Advisory Committee for Aeronautics
Cleveland, Ohio, November 17, 1953

3083

APPENDIX - SYMBOLS

The following symbols are used in this report:

D	percent of distance from hub to shroud
f_s	slip factor, ratio of absolute tangential velocity at exit to impeller speed at exit, taken herein as ratio of over-all enthalpy rise to U^2/gJ
g	acceleration due to gravity
ΔH_{ad}	isentropic enthalpy rise relative to impeller
ΔH_{act}	actual enthalpy rise relative to impeller, based on impeller speed
J	mechanical equivalent of heat
n	distance along normal to streamline
P	absolute total pressure
P_0	stagnation pressure at impeller inlet
P_r	relative total pressure
ΔP_r	difference between theoretical relative total pressure and measured relative total pressure
p	static pressure
Q	ratio of flow velocity relative to impeller to velocity of sound at inlet stagnation condition
q	velocity relative to impeller
R	radius, in.
r	radius
r_c	radius of curvature, positive for concave curvature in direction of rotation
s	distance along streamline
t	time

U	impeller tip speed
u	tangential component of velocity relative to impeller, positive in direction of rotation
v	radial component of velocity, positive in outward direction
W	weight flow, lb/sec
β	blade angle or flow direction (shown in fig. 21), positive for forward-curved blades
δ	ratio of stagnation pressure at inlet to standard sea-level pressure
η_{ad}	over-all adiabatic efficiency
$\eta_{ad,rel}$	relative adiabatic efficiency, ratio of ΔH_{ad} to ΔH_{act}
θ	ratio of inlet stagnation temperature to standard sea-level temperature
θ'	angular displacement of fluid relative to impeller, positive in direction of rotation
ρ	mass density
ω	angular velocity of impeller, radians/sec

REFERENCES

1. Stanitz, John D., and Ellis, Gaylord O.: Two-Dimensional Compressible Flow in Centrifugal Compressors with Straight Blades. NACA Rep. 954, 1950. (Supersedes NACA TN 1932.)

2. Stanitz, John D., and Prian, Vasily D.: A Rapid Approximate Method for Determining Velocity Distribution on Impeller Blades of Centrifugal Compressors. NACA TN 2421, 1951.

3. Hamrick, Joseph T., Ginsburg, Ambrose, and Osborn, Walter M.: Method of Analysis for Compressible Flow Through Mixed-Flow Centrifugal Impellers of Arbitrary Design. NACA Rep. 1082, 1952. (Supersedes NACA TN 2165.)

4. Ellis, Gaylord O., and Stanitz, John D.: Comparison of Two- and Three-Dimensional Potential-Flow Solutions in a Rotating Impeller Passage. NACA TN 2806, 1952.

5. Stanitz, John D.: Approximate Design Method for High-Solidity Blade Elements in Compressors and Turbines. NACA TN 2408, 1951.

6. Kramer, James J., and Stanitz, John D.: A Note on Secondary Flow in Rotating Radial Channels. NACA TN 3013, 1953.

7. Michel, Donald J., Ginsburg, Ambrose, and Mizisin, John: Experimental Investigation of Flow in the Rotating Passages of a 48-Inch Impeller at Low Speeds. NACA RM E51D20, 1951.

8. Michel, Donald J., Mizisin, John, and Prian, Vasily D.: Effect of Changing Passage Configuration on Internal-Flow Characteristics of a 48-Inch Centrifugal Compressor. I - Change in Blade Shape. NACA TN 2706, 1952.

9. Prian, Vasily D., and Michel, Donald J.: An Analysis of Flow in Rotating Passage of Large Radial-Inlet Centrifugal Compressor at Tip Speed of 700 Feet Per Second. NACA TN 2584, 1951.

10. Mizisin, John, and Michel, Donald J.: Effect of Changing Passage Configuration on Internal-Flow Characteristics of a 48-Inch Centrifugal Compressor. II - Change in Hub Shape. NACA TN 2835, 1952.

11. Hansen, Arthur G., Herzig, Howard Z., and Costello, George R.: A Visualization Study of Secondary Flows in Cascades. NACA TN 2947, 1953.

3083

12. Hamrick, Joseph T., and Mizisin, John: Investigation of Flow Fluctuations at the Exit of a Radial-Flow Centrifugal Impeller. NACA RM E52H11, 1952.

13. Benser, William A., and Moses, Jason J.: An Investigation of Backflow Phenomenon in Centrifugal Compressors. NACA Rep. 806, 1945. (Supersedes NACA WR E-8.)

14. Huppert, Merle C., and Benser, William A.: Some Stall and Surge Phenomena in Axial-Flow Compressors. Paper presented at Twenty-First Inst. Aero. Sci. meeting, New York (N.Y.), Jan. 26-29, 1953.

15. Stodola, A.: Steam and Gas Turbines. Vol. II. McGraw-Hill Book Co., Inc., 1927, p. 986. (Reprinted, Peter Smith (New York), 1945.)

16. King, Austin, and Glodeck, Edward: Performance Characteristics of Mixed-Flow Impeller and Vaned Diffuser with Several Modifications. NACA MR E-197, 1942.

17. Martinuzzi, P. F.: German Supercharger Tests. Flight, vol. 37, no. 1627, Feb. 29, 1940, pp. 194e-194h. (See also vol. 37, no. 1631, Mar. 28, 1940, pp. 295a-295c.)

18. Ritter, William K., and Johnsen, Irving A.: Performance Effect of Fully Shrouding a Centrifugal Supercharger Impeller. NACA WR E-2, 1945. (Supersedes NACA ARR E5H23.)

3083

CM-3

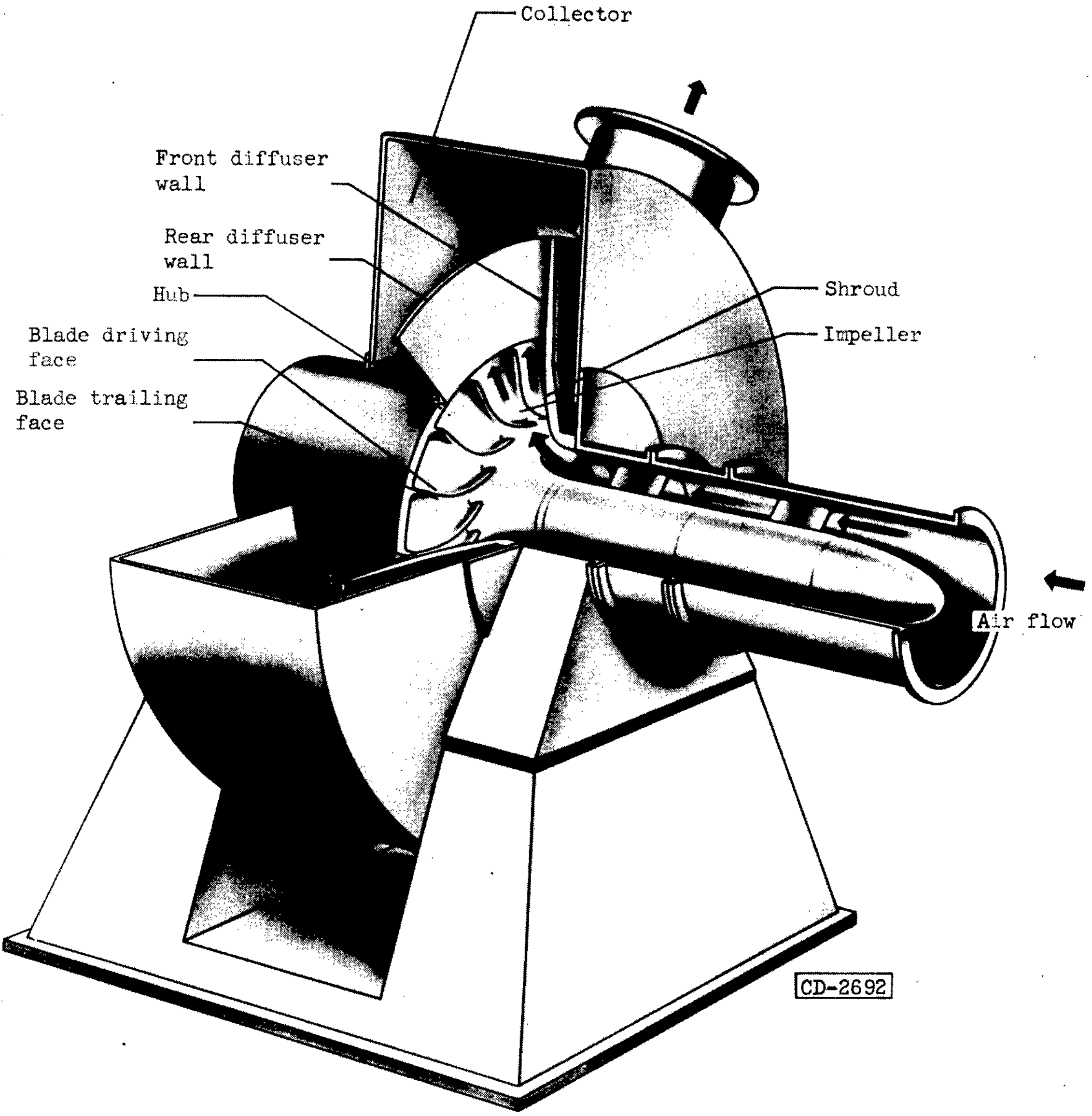

Figure 1. - 48-Inch impeller test rig.

3083

CM-3 back

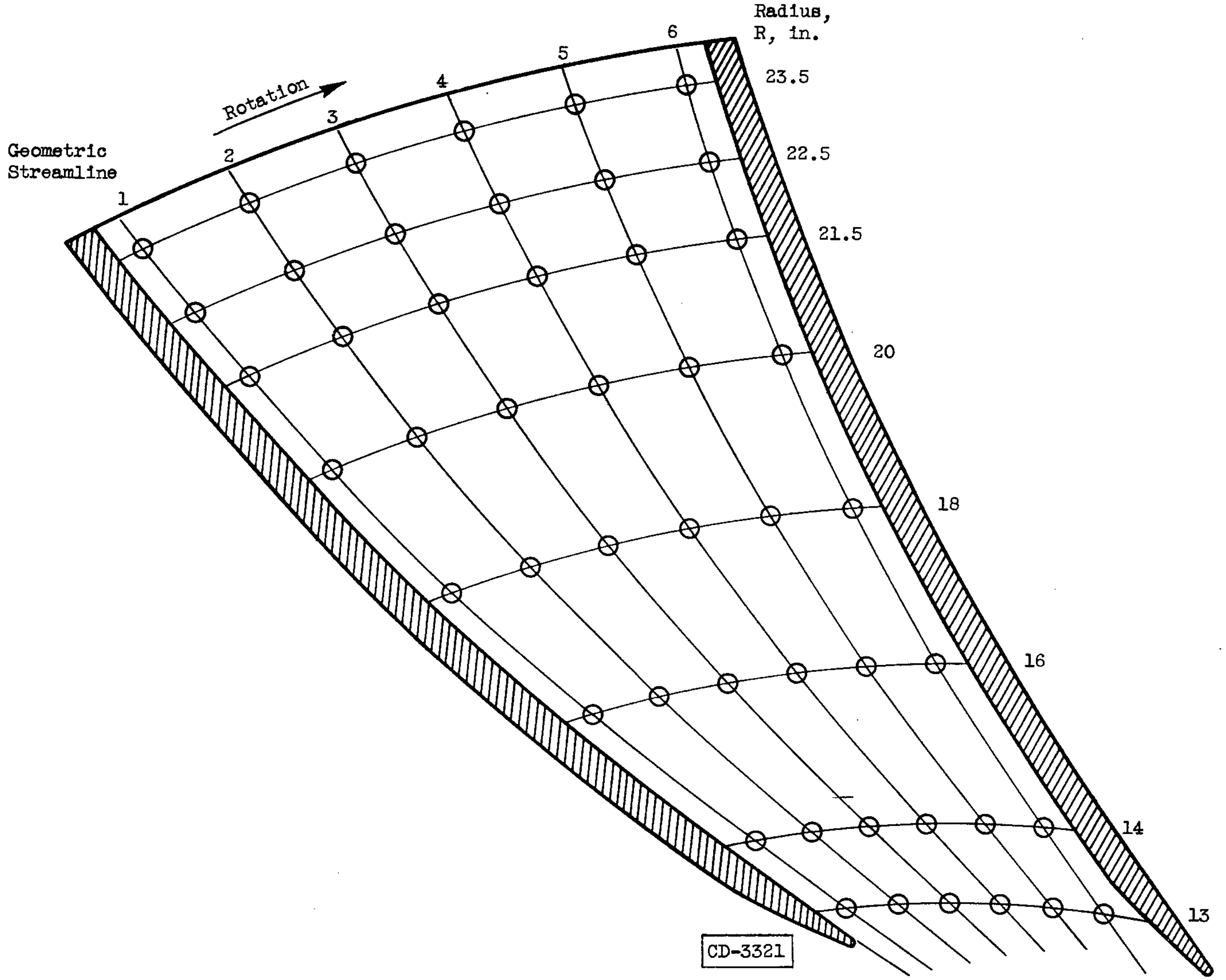

Figure 2. - Total-pressure probe and static-pressure tap locations in blade-to-blade plane.

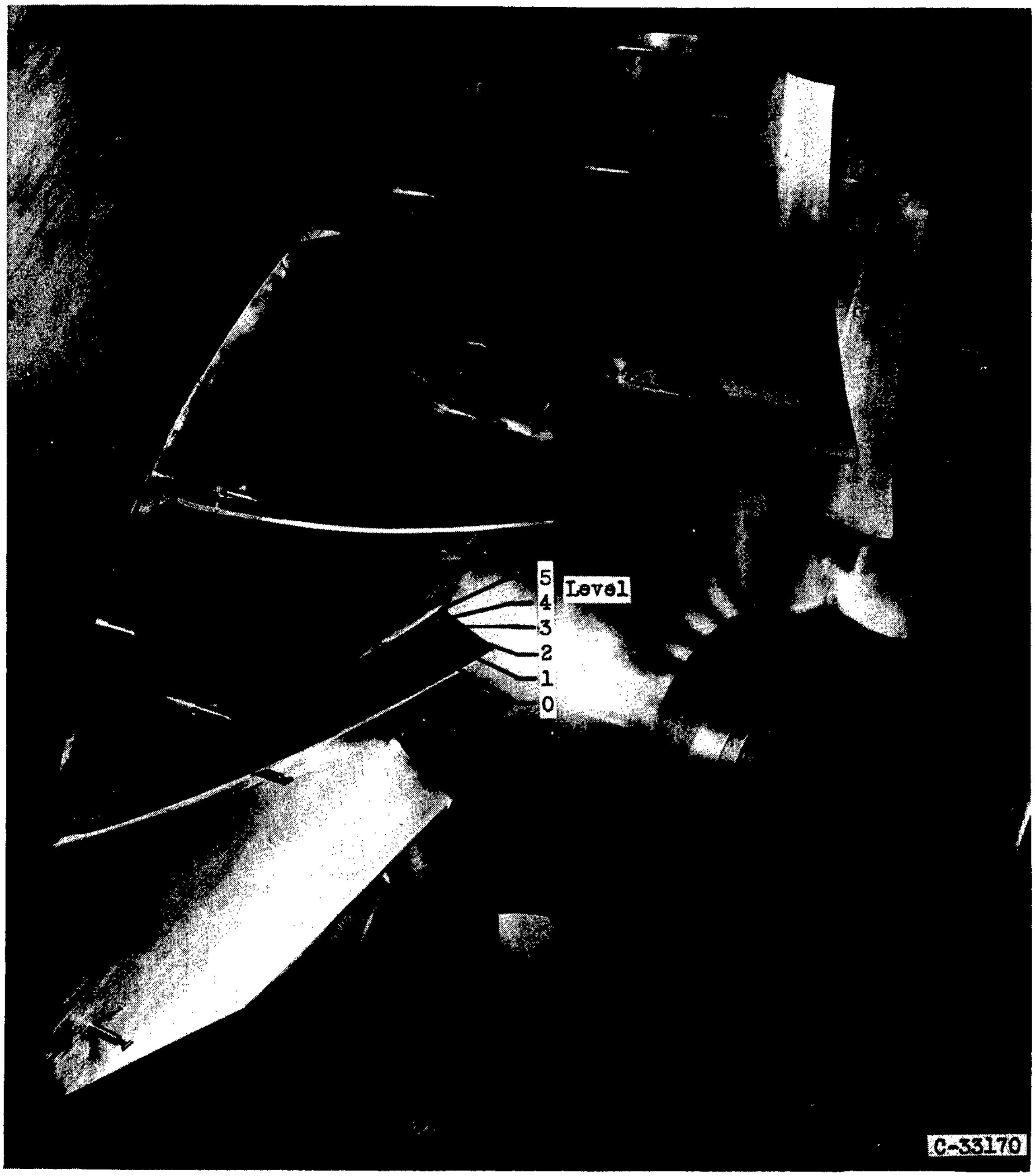

Figure 3. - Photograph of instrumented impeller showing instrument levels.

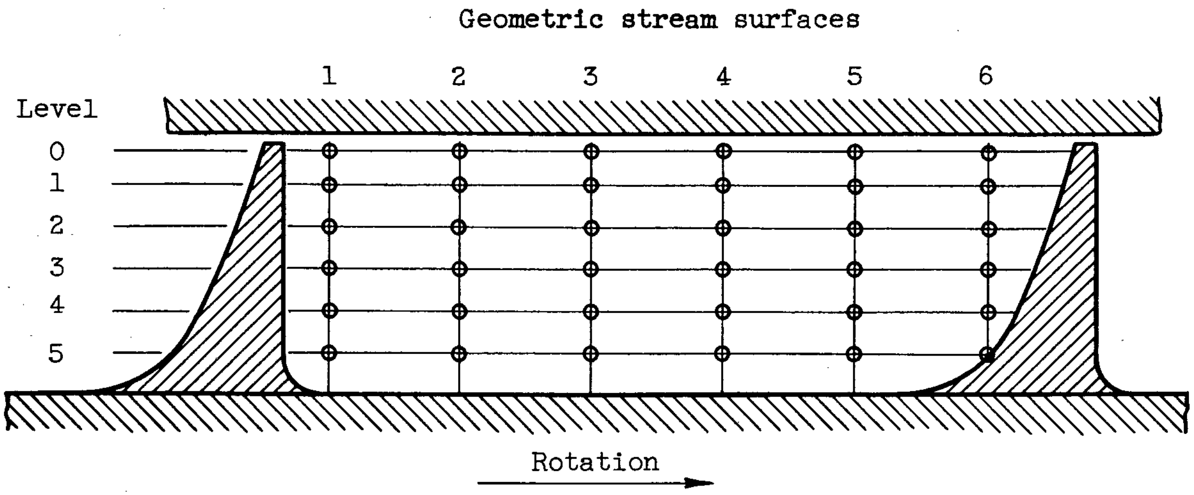

Figure 4. - Total-pressure probe locations for typical passage cross section.

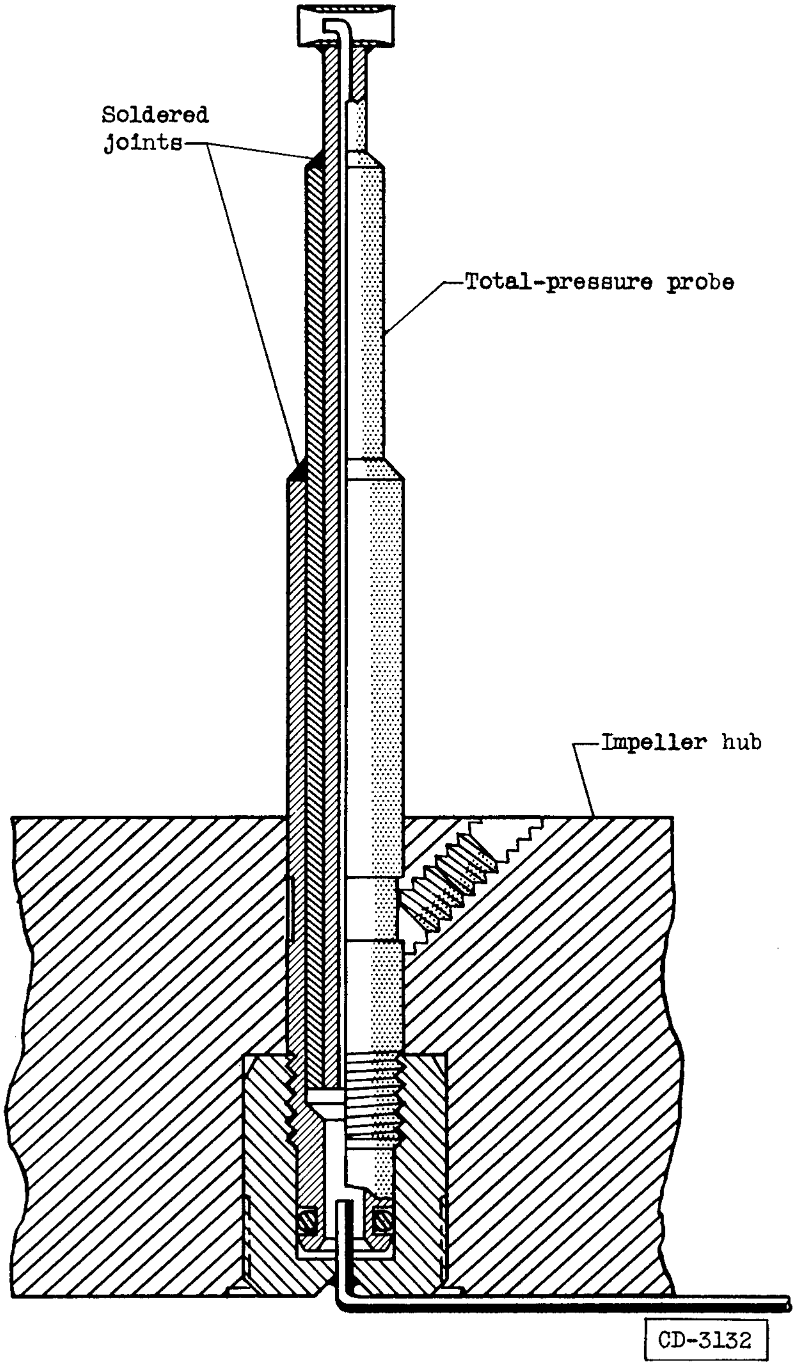

Figure 5. - Schematic diagram of telescoping total-pressure probe used for all levels.

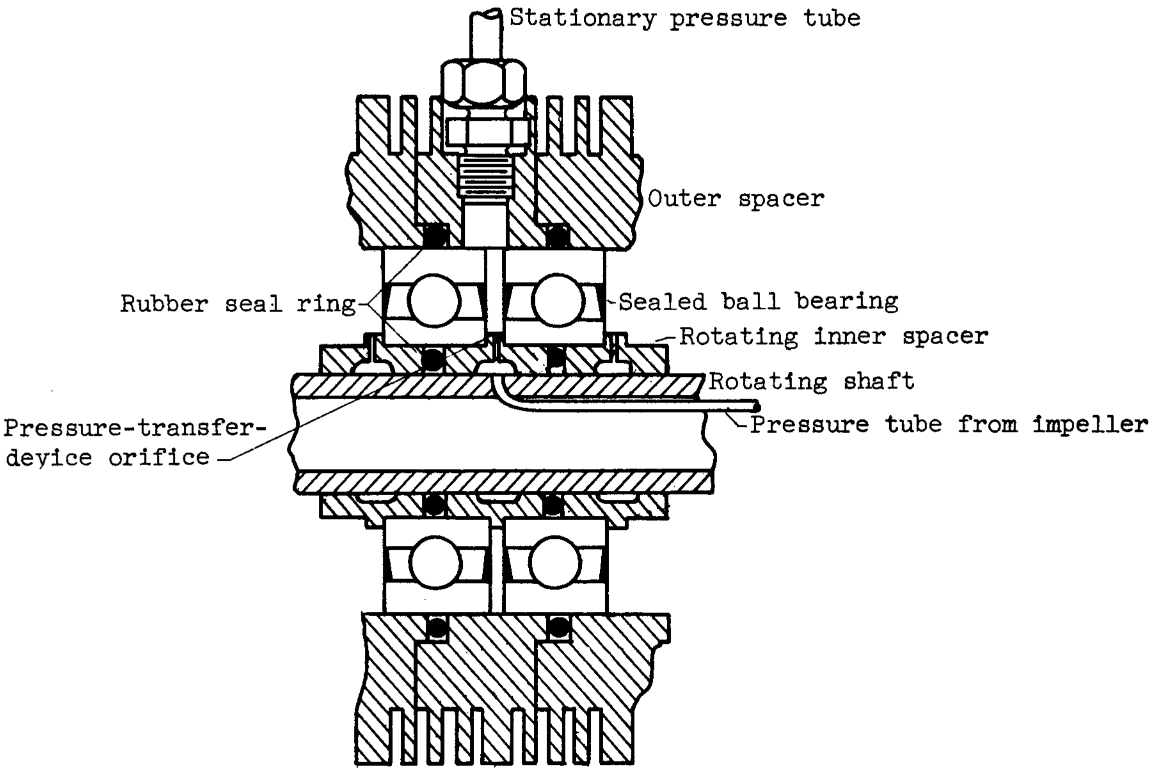

Figure 6. - Section of pressure-transfer device.

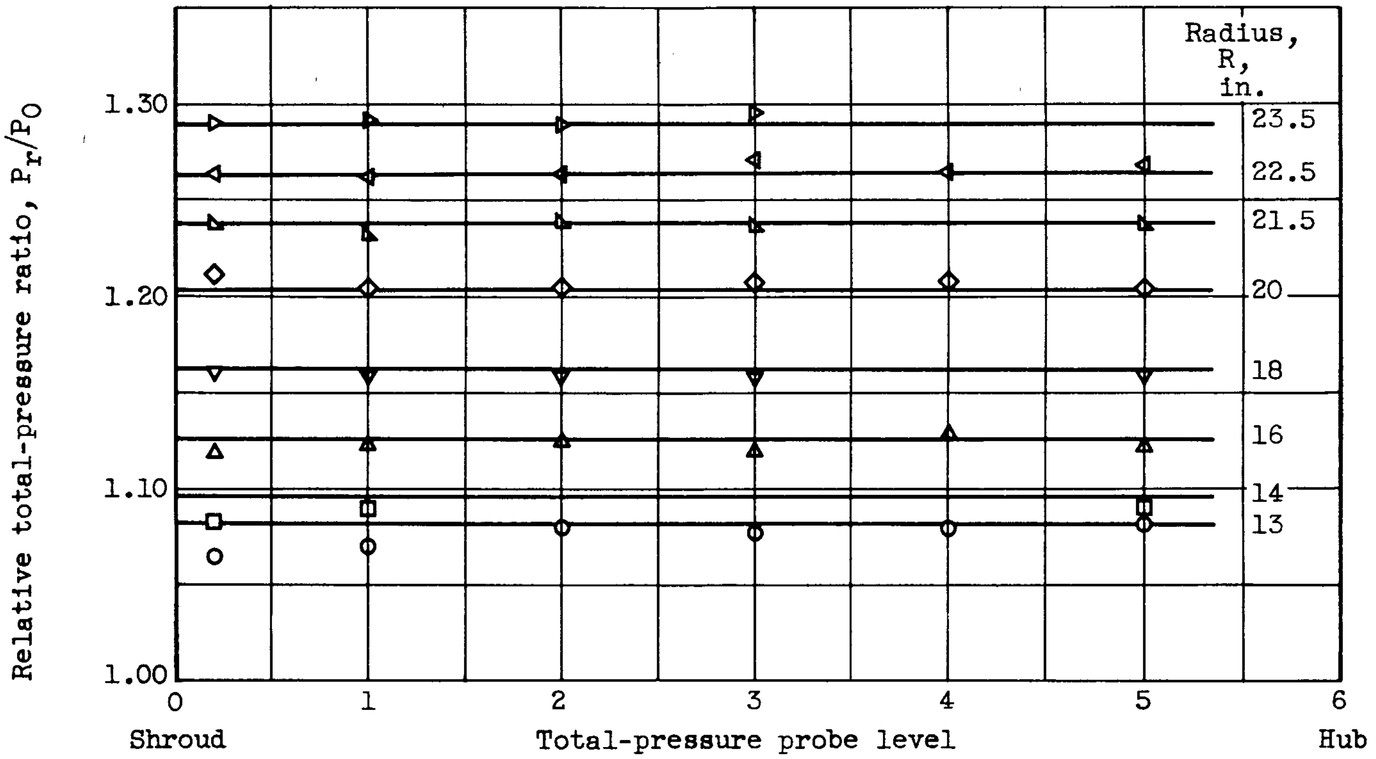

Figure 7. - Total-pressure ratios on stream surface nearest to blade driving face (geometric streamline 1) for $W\sqrt{\theta}/\delta$ of 29.3 pounds per second. Solid lines show theoretical value at each radius.

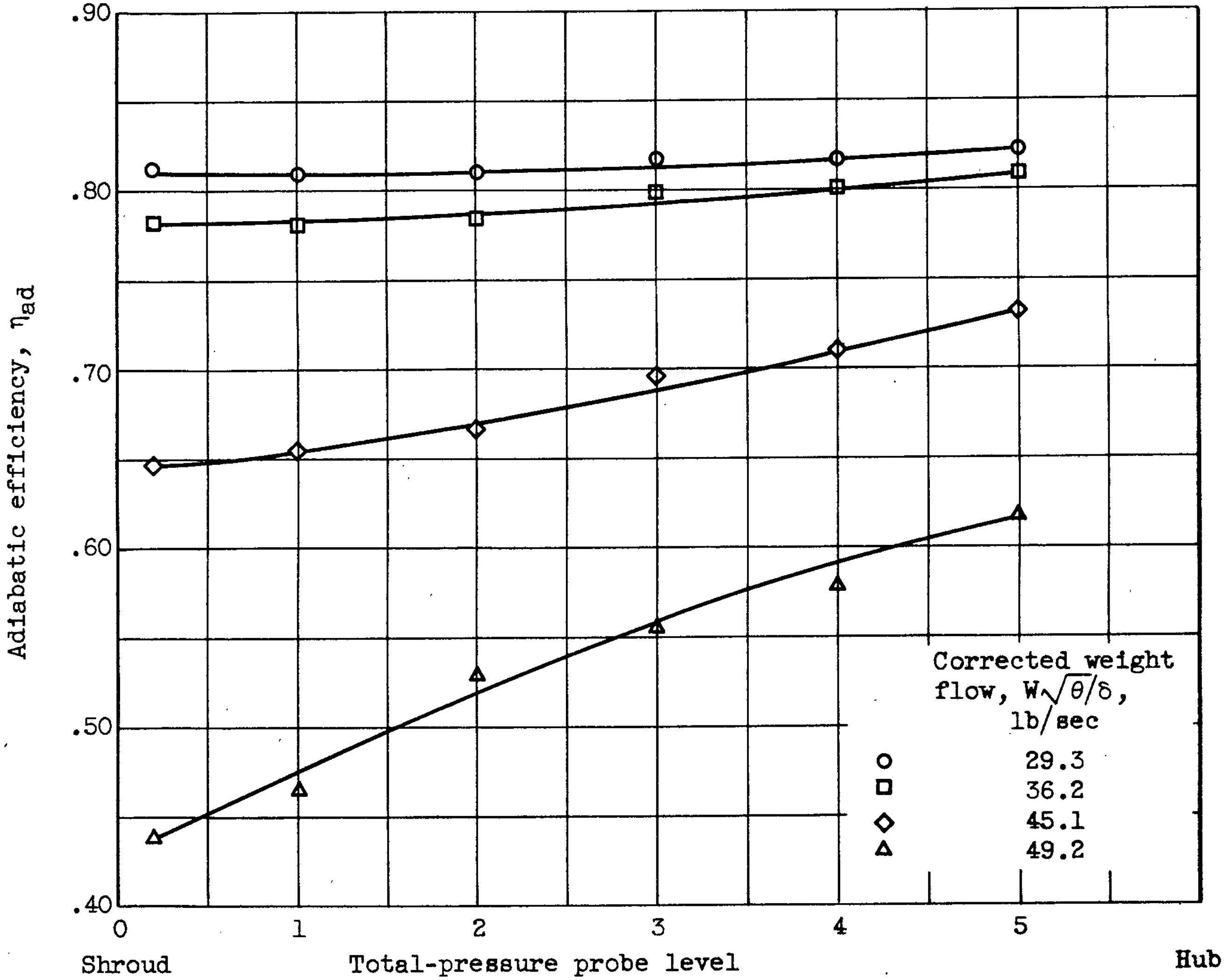

Figure 8. - Change in over-all efficiency with changing probe height for several weight flows. (Maximum probe height is at level 0.)

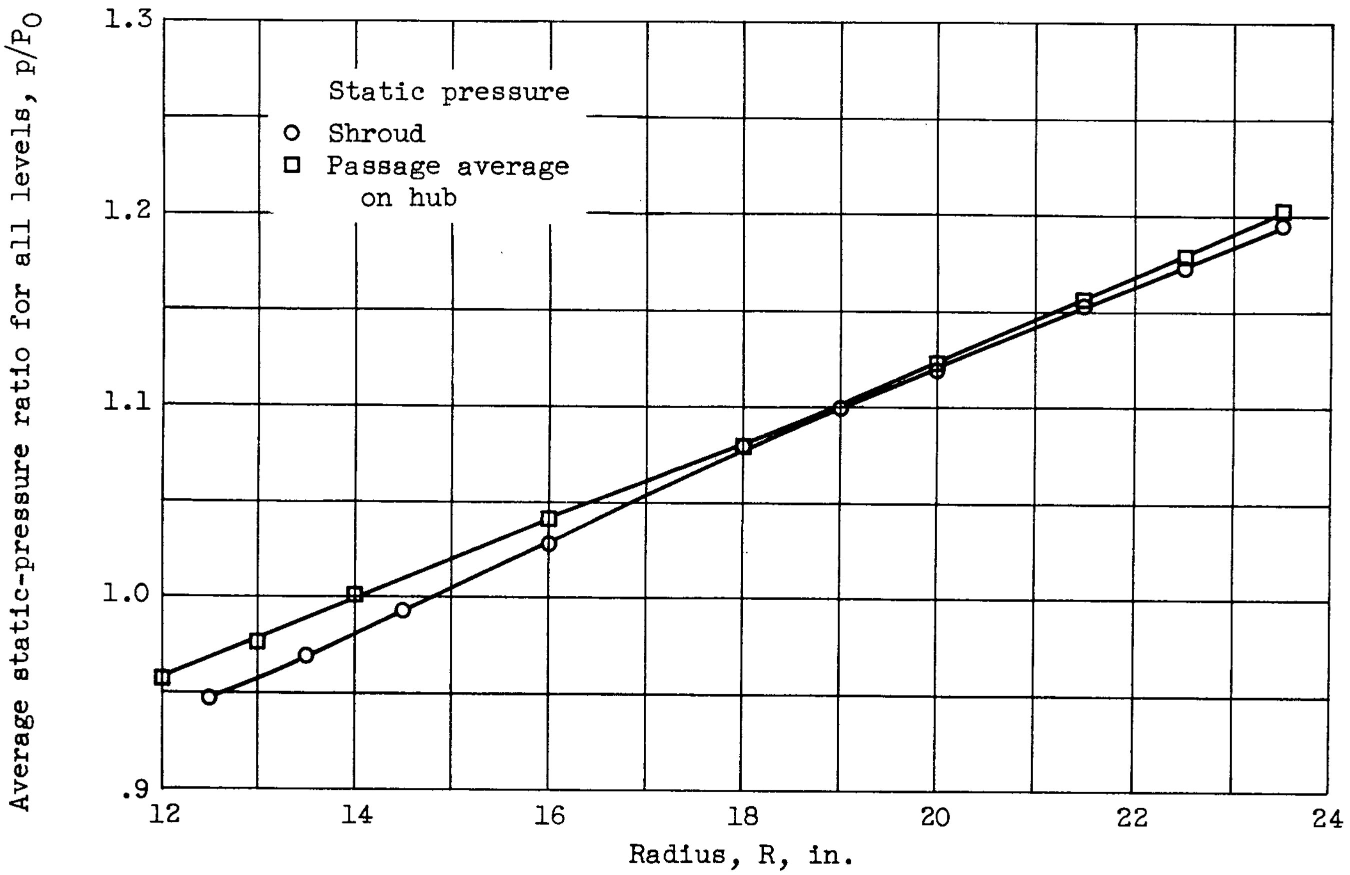

Figure 9. - Comparison of static-pressure ratio along impeller hub and stationary shroud for $W\sqrt{\theta}/\delta$ of 29.3 pounds per second.

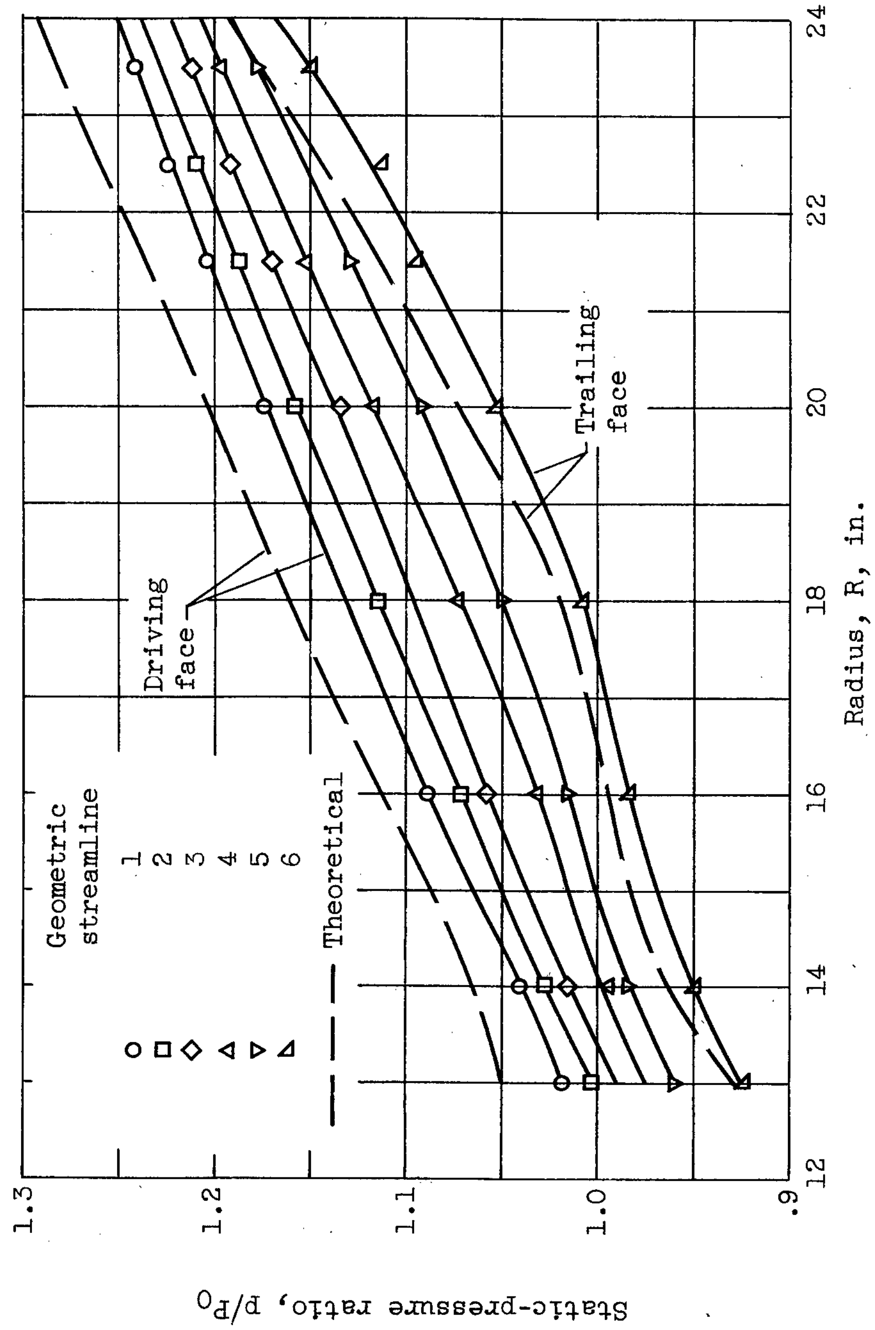

Figure 10. - Experimental static-pressure distribution and comparison of theoretical with experimental near blade faces for $W\sqrt{\theta}/\delta$ of 29.3 pounds per second.

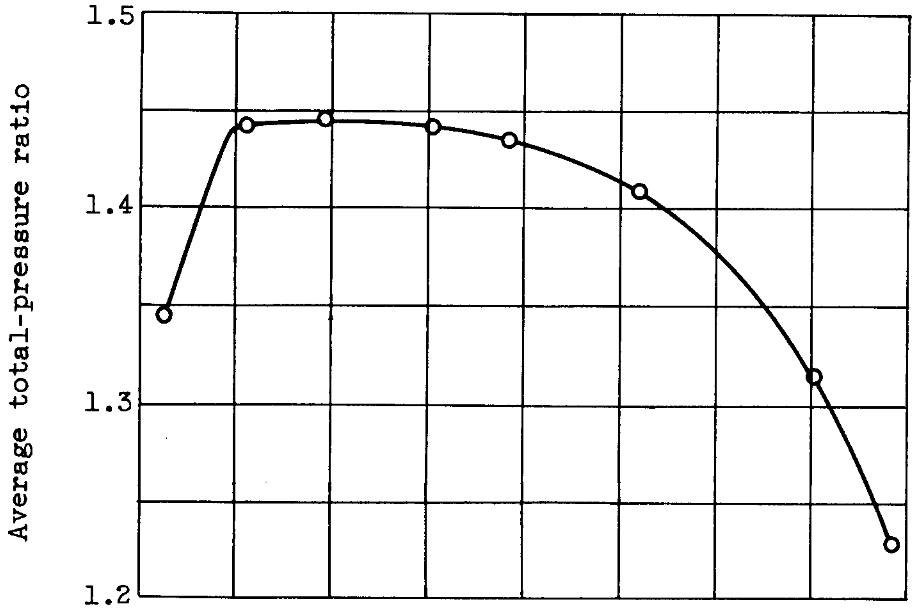

(a) Over-all pressure ratio.

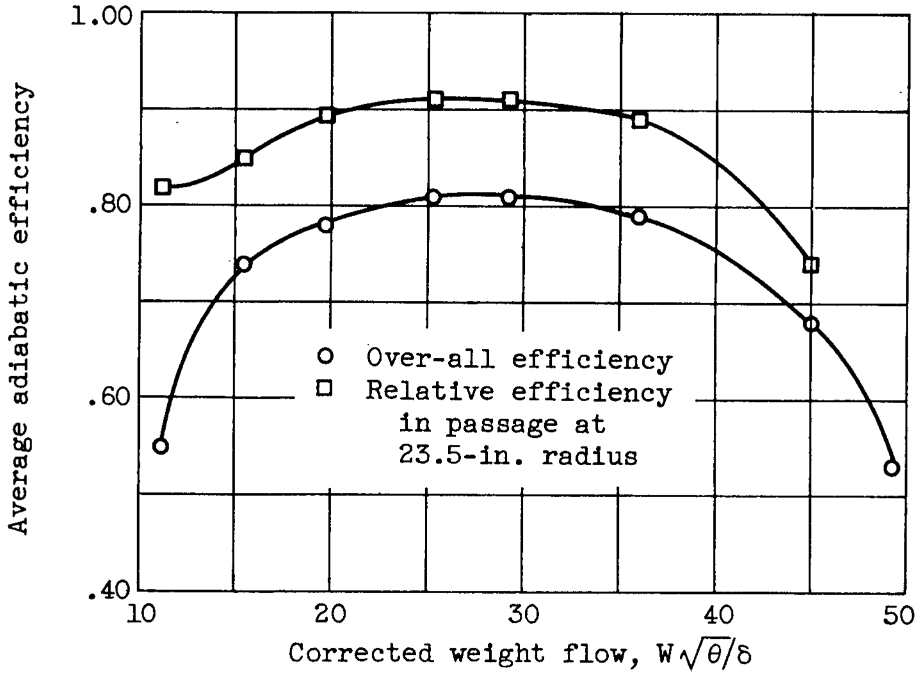

(b) Adiabatic efficiency.

Figure 11. - Average performance at equivalent tip speed of 700 feet per second.

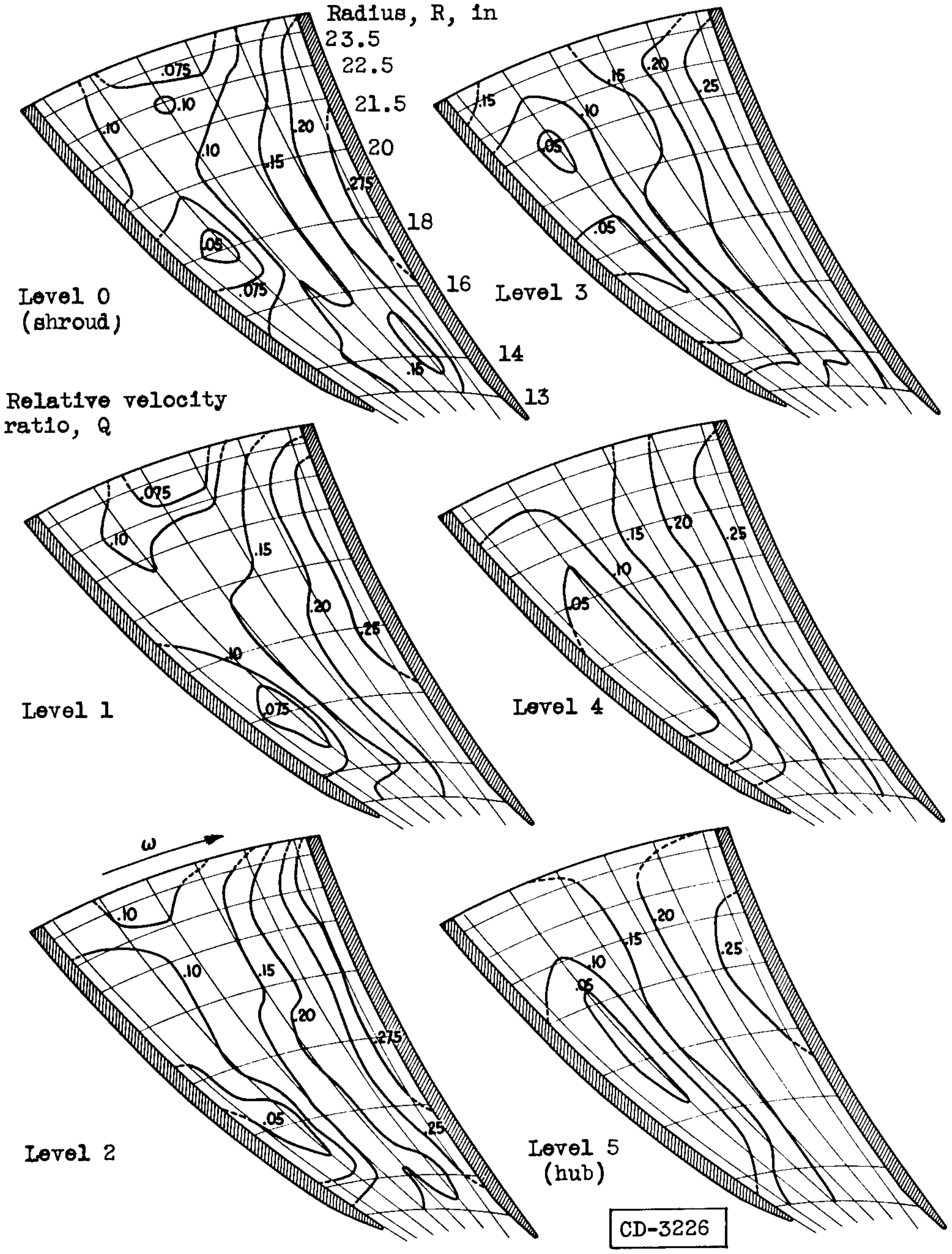

(a) Relative velocity distribution.

Figure 12. - Flow characteristics in rotating passage for six levels between hub and shroud at corrected weight flow of 11.2 pounds per second.

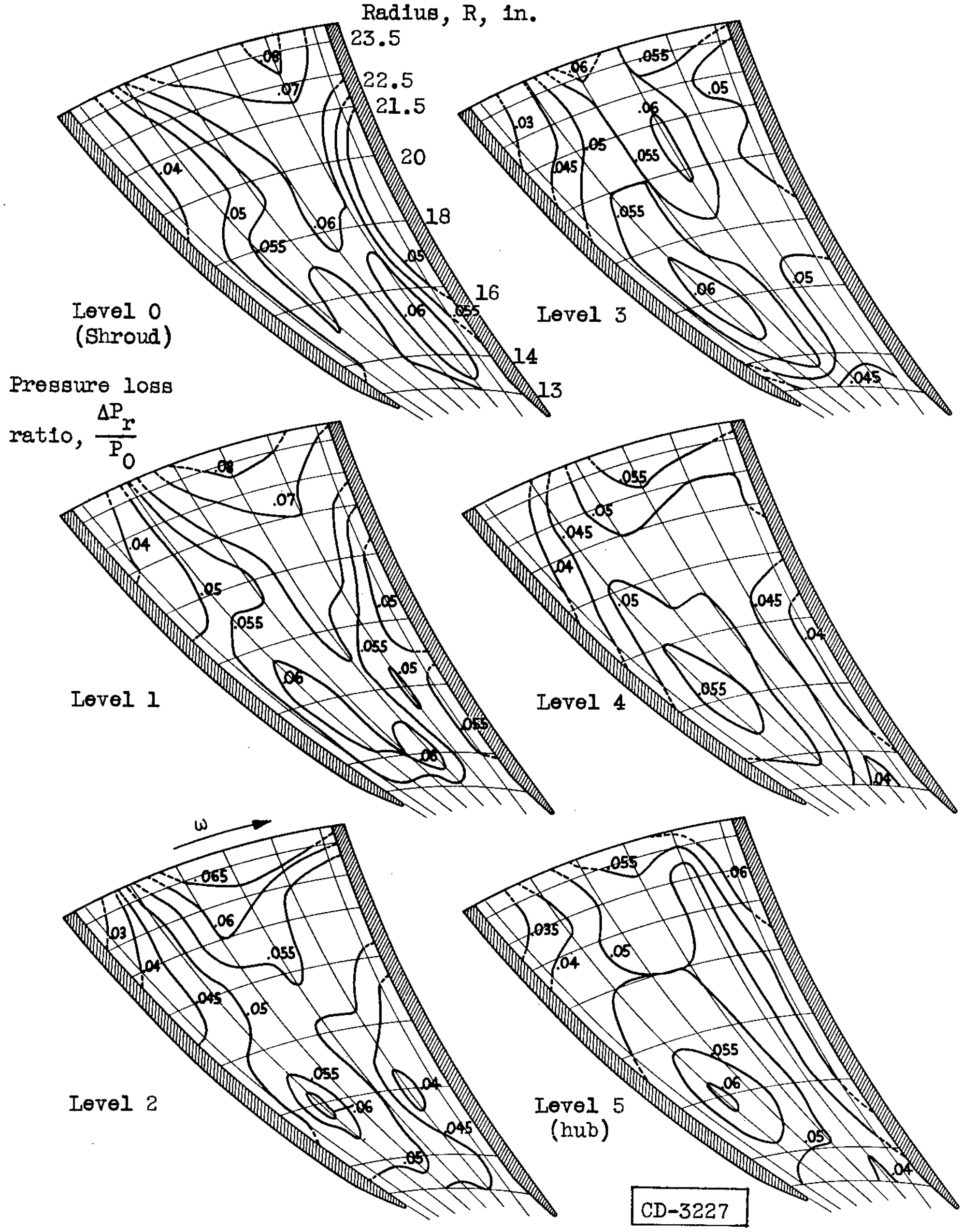

(b) Total-pressure-loss distribution.

Figure 12. - Continued. Flow characteristics in rotating passage for six levels between hub and shroud at corrected weight flow of 11.2 pounds per second.

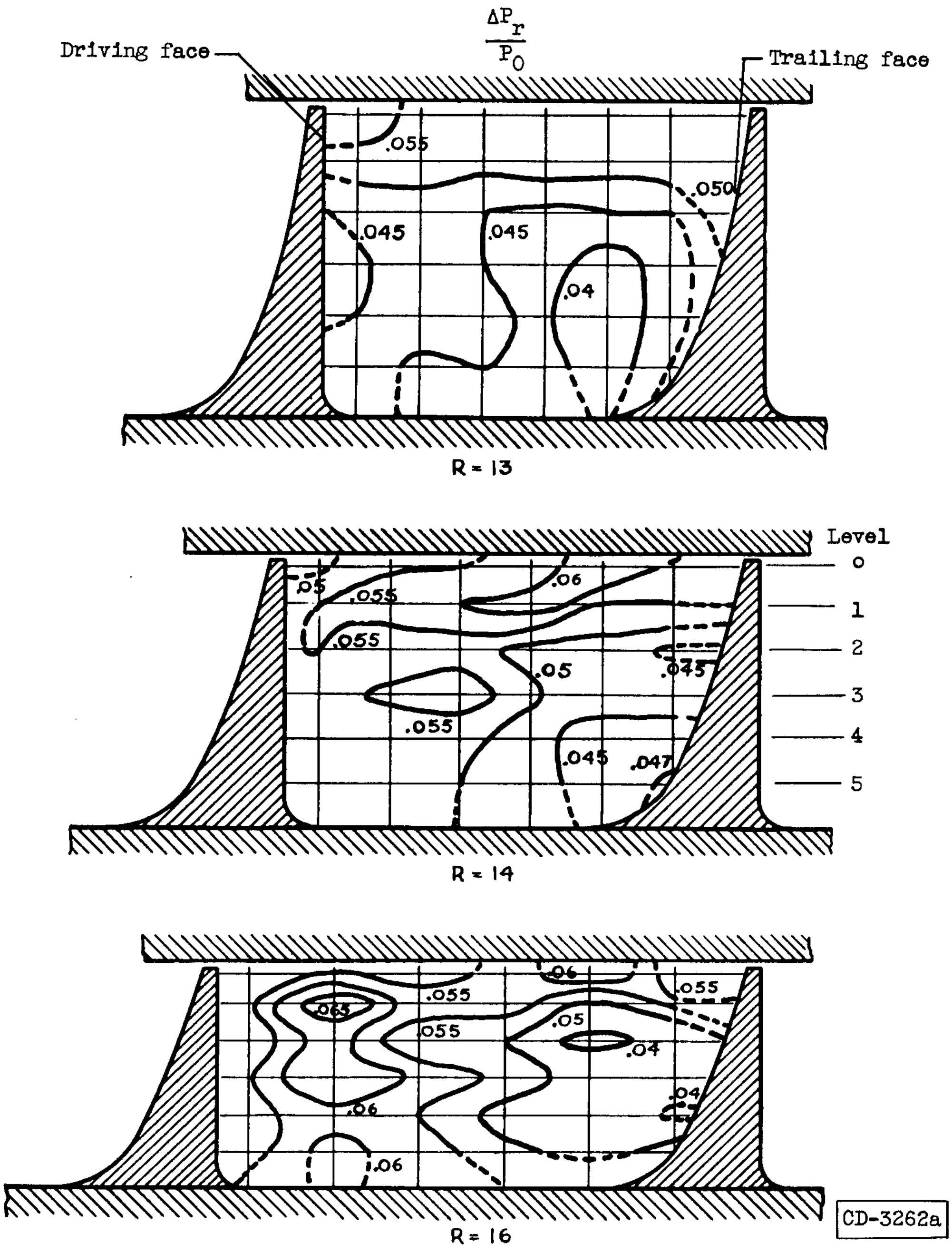

(c) Cross-sectional view of total-pressure-loss distribution.

Figure 12. - Continued. Flow characteristics in rotating passage for six levels between hub and shroud at corrected weight flow of 11.2 pounds per second.

3083

CM-5

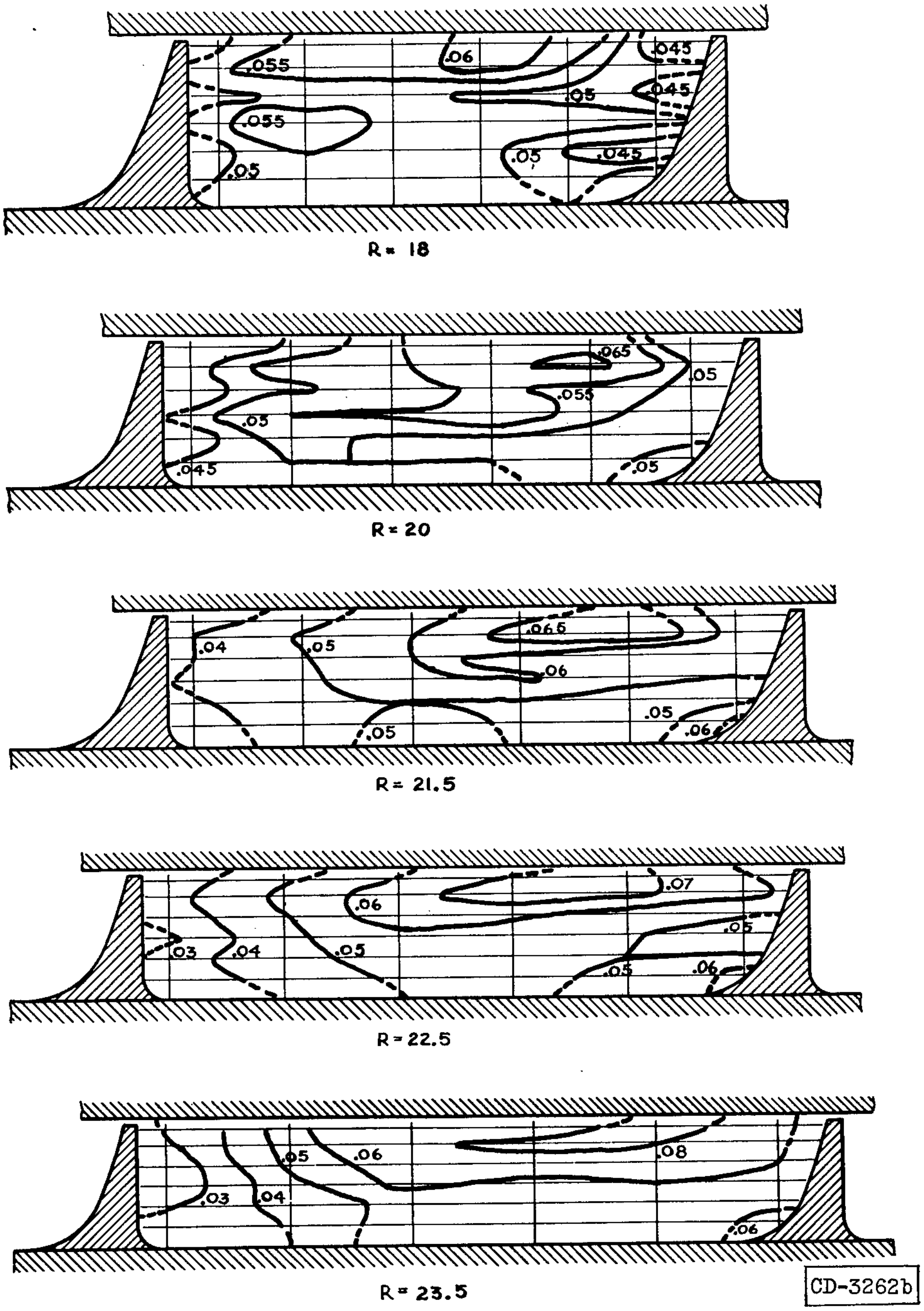

(c) Concluded. Cross-sectional view of total-pressure-loss distribution.

Figure 12. - Concluded. Flow characteristics in rotating passage for six levels between hub and shroud at corrected weight flow of 11.2 pounds per second.

3083

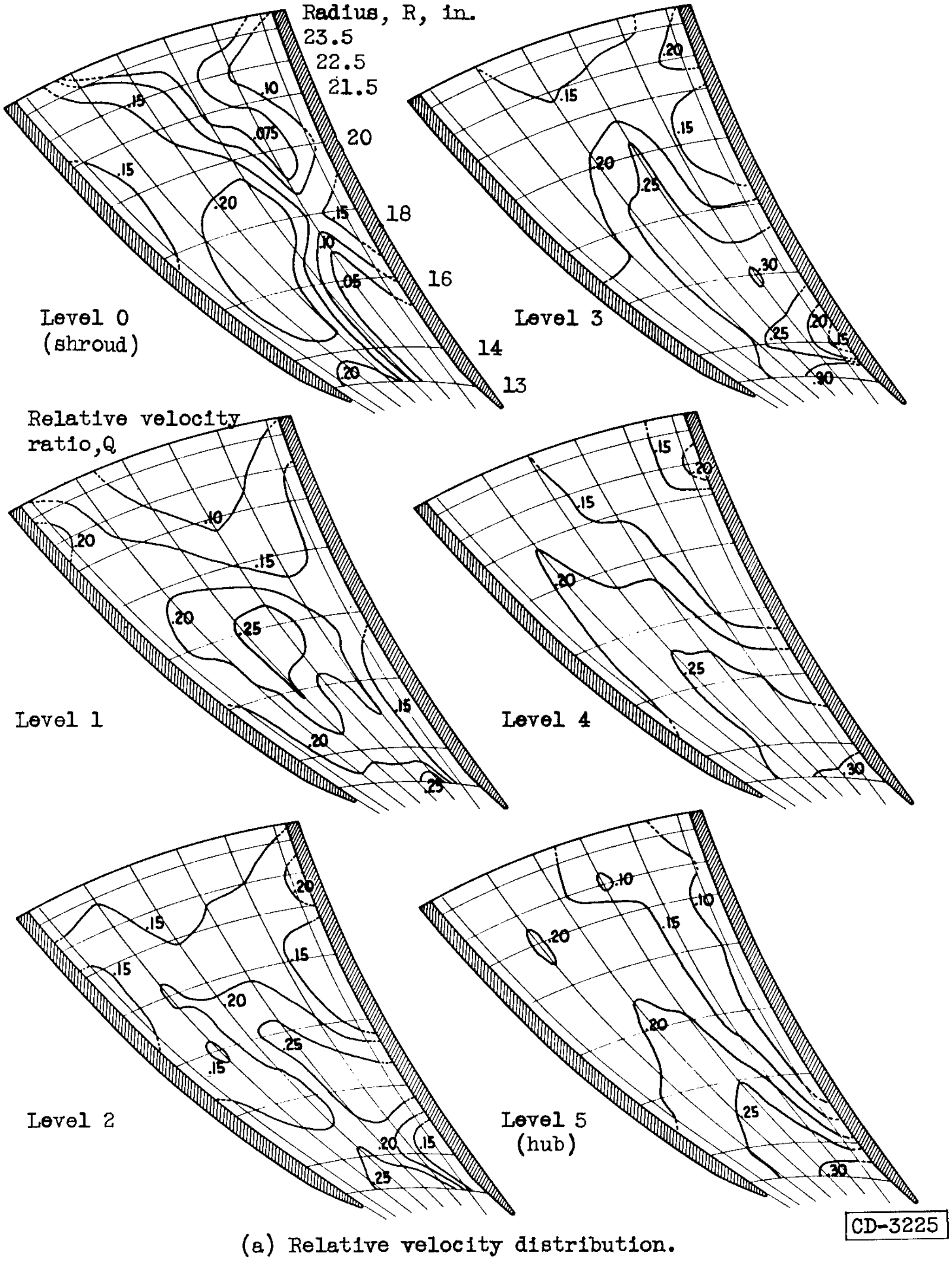

(a) Relative velocity distribution.

Figure 13. - Flow characteristics in rotating passage for six levels between hub and shroud at corrected weight flow of 15.6 pounds per second.

3083

CM-5 back

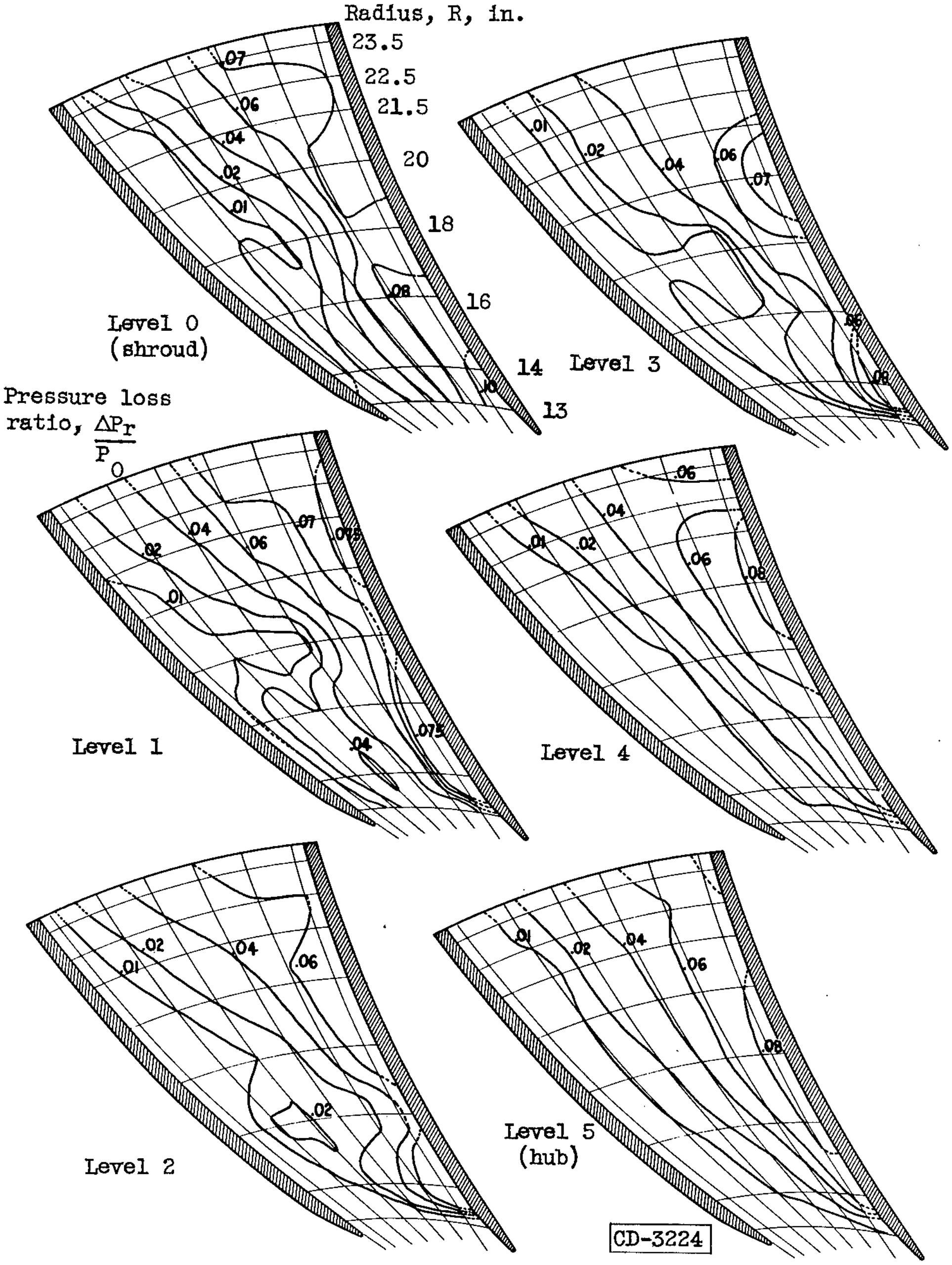

(b) Total-pressure-loss distribution.

Figure 13. - Continued. Flow characteristics in rotating passage for six levels between hub and shroud at corrected weight flow of 15.6 pounds per second.

3083

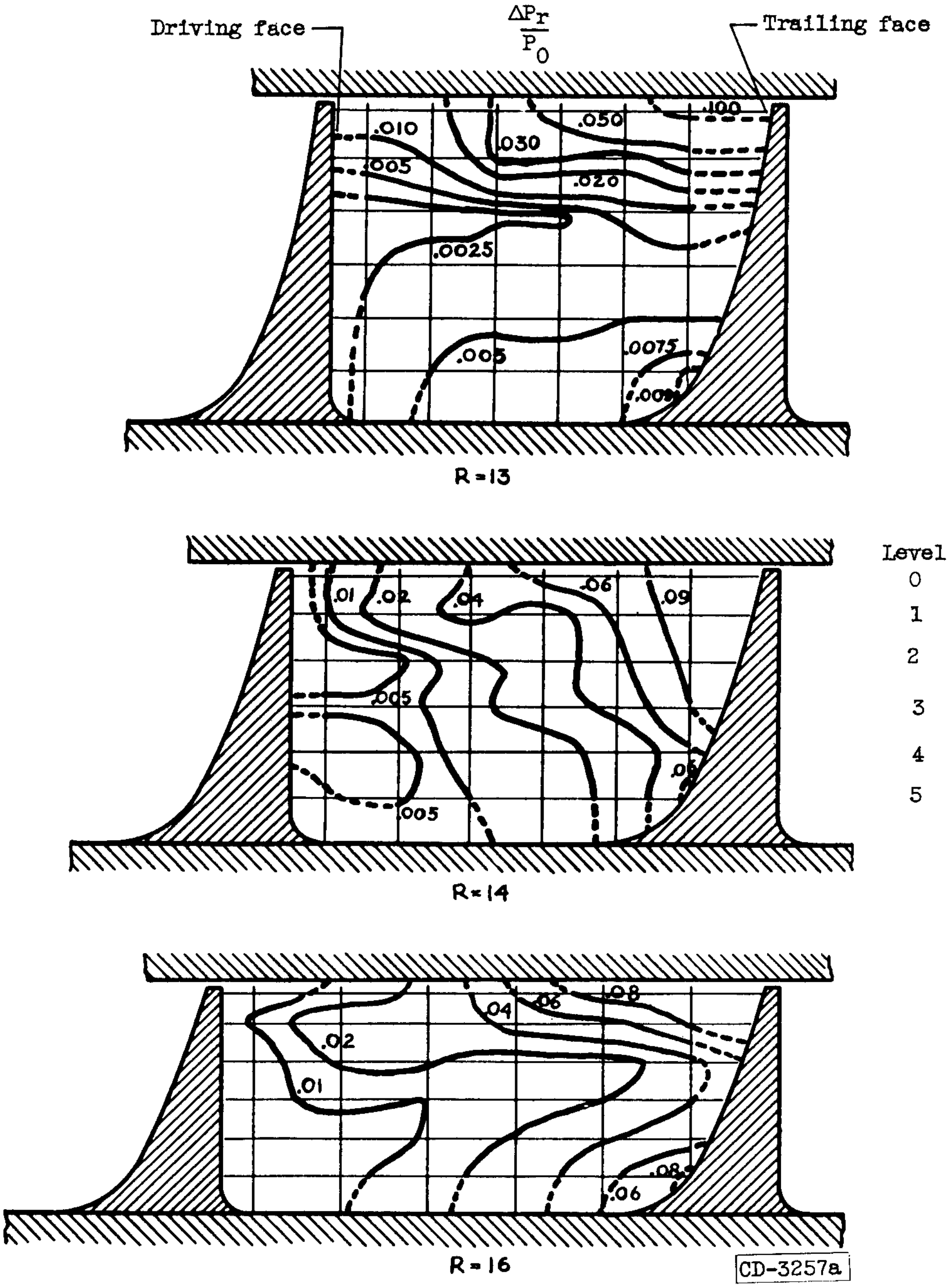

(c) Cross-sectional view of total-pressure-loss distribution.

Figure 13. - Continued. Flow characteristics in rotating passage for six levels between hub and shroud at corrected weight flow of 15.6 pounds per second.

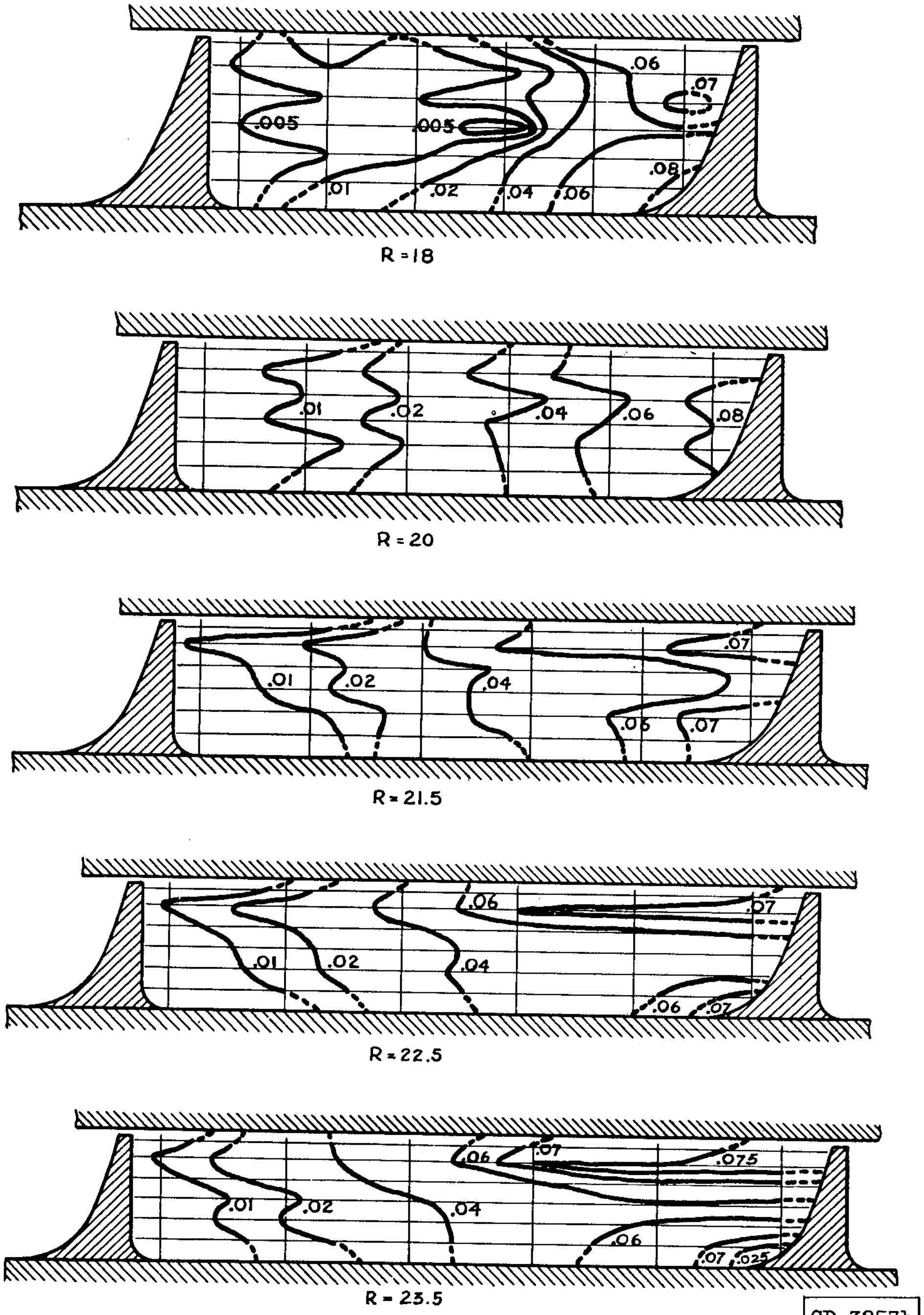

CD-3257b

(c) Concluded. Cross-sectional view of total-pressure-loss distribution.

Figure 13. - Concluded. Flow characteristics in rotating passage for six levels between hub and shroud at corrected weight flow of 15.6 pounds per second.

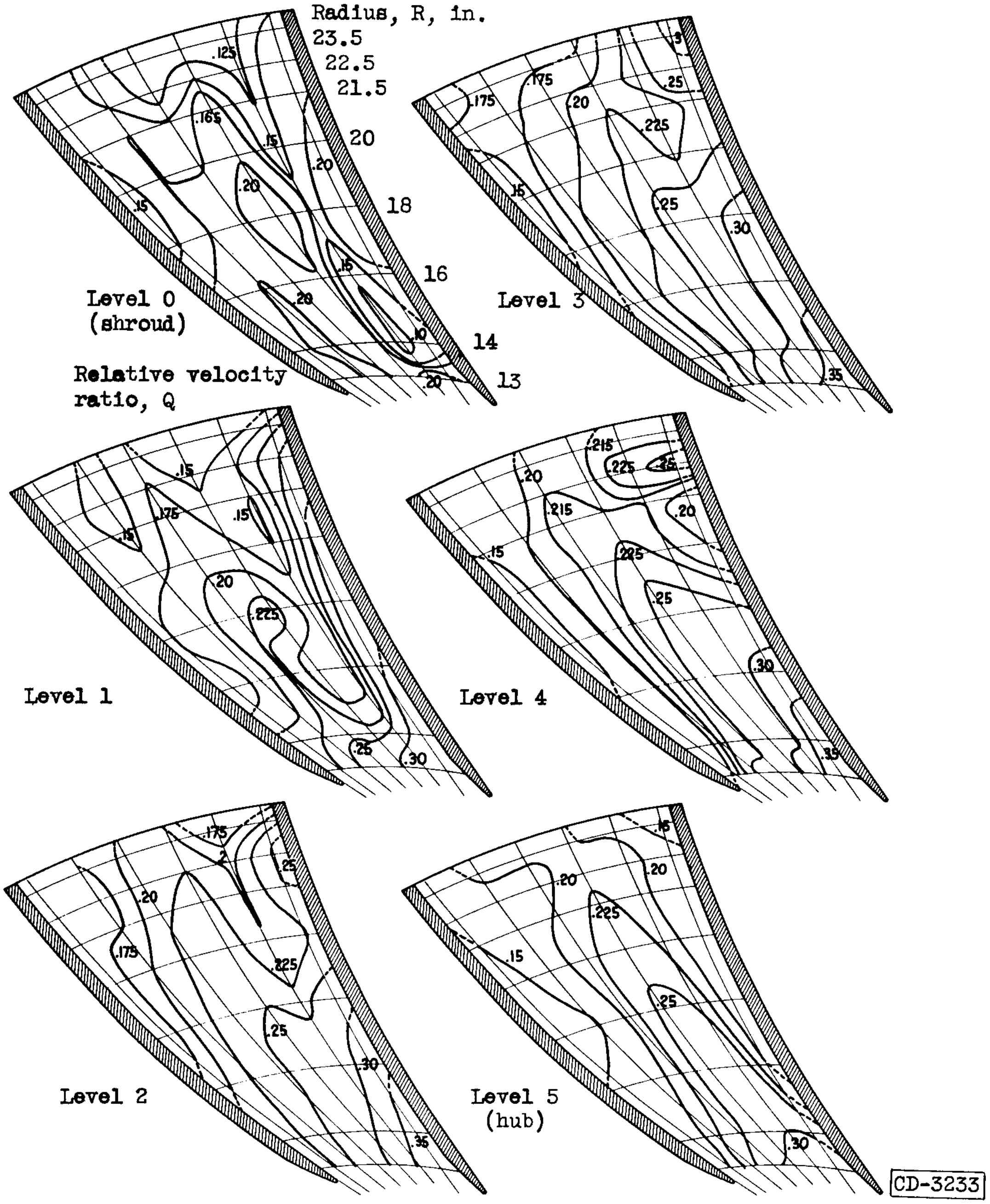

(a) Relative velocity distribution.

Figure 14. - Flow characteristics in rotating passage for six levels between hub and shroud at corrected weight flow of 19.6 pounds per second.

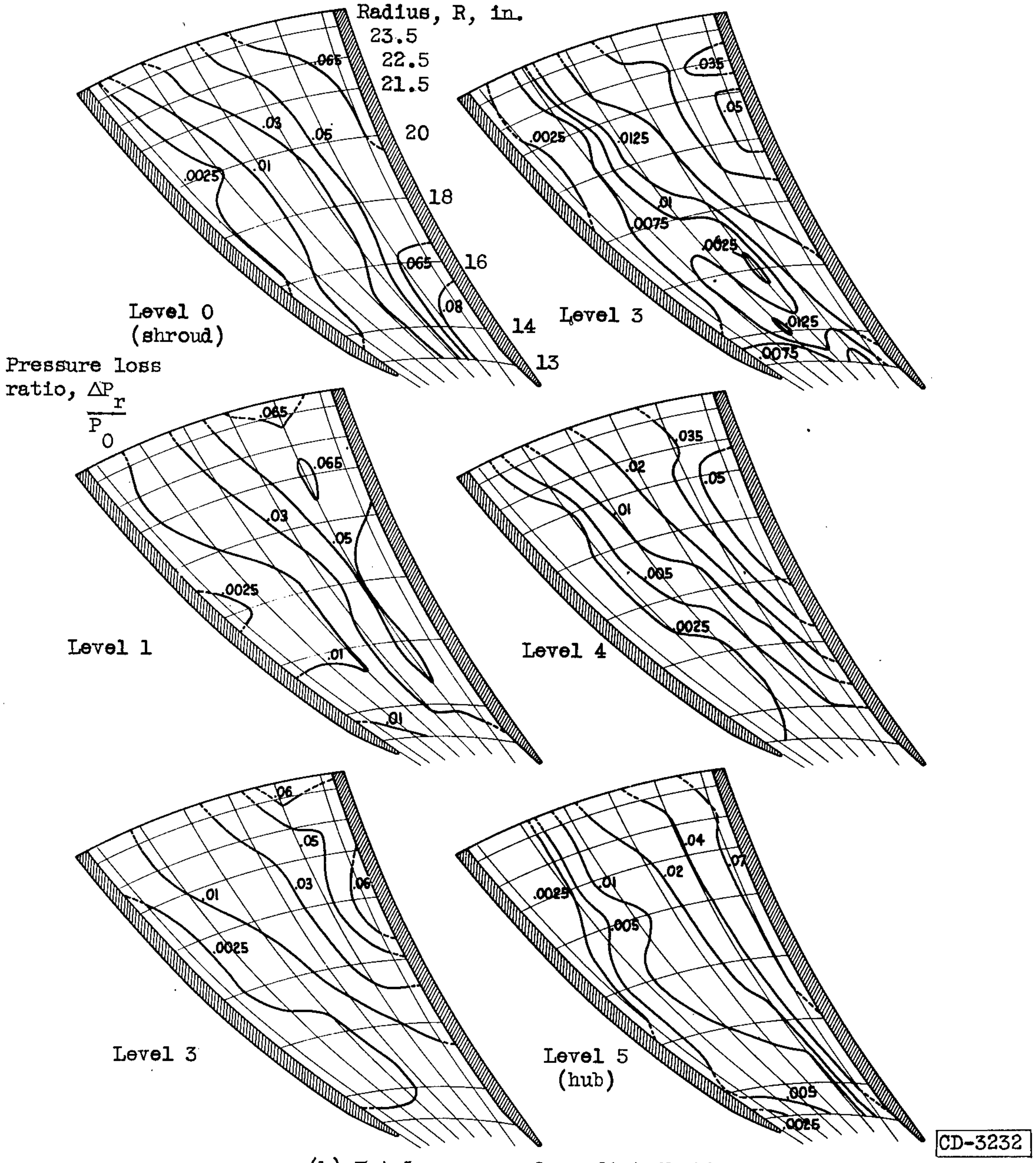

(b) Total-pressure-loss distribution.

Figure 14. - Continued. Flow characteristics in rotating passage for six levels between hub and shroud at corrected weight flow of 19.6 pounds per second.

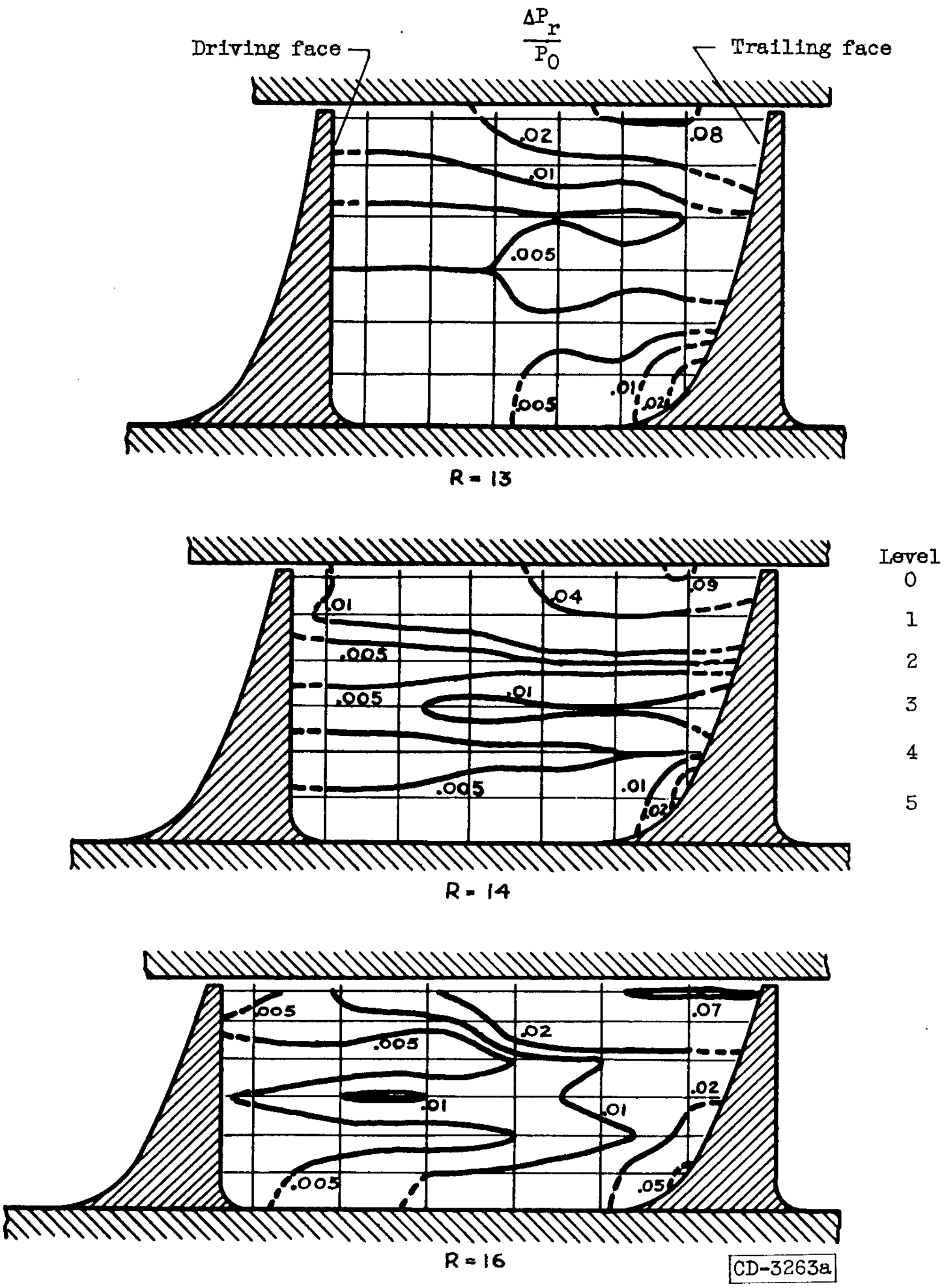

(c) Cross-sectional view of total-pressure-loss distribution.

Figure 14. - Continued. Flow characteristics in rotating passage for six levels between hub and shroud at corrected weight flow of 19.6 pounds per second.

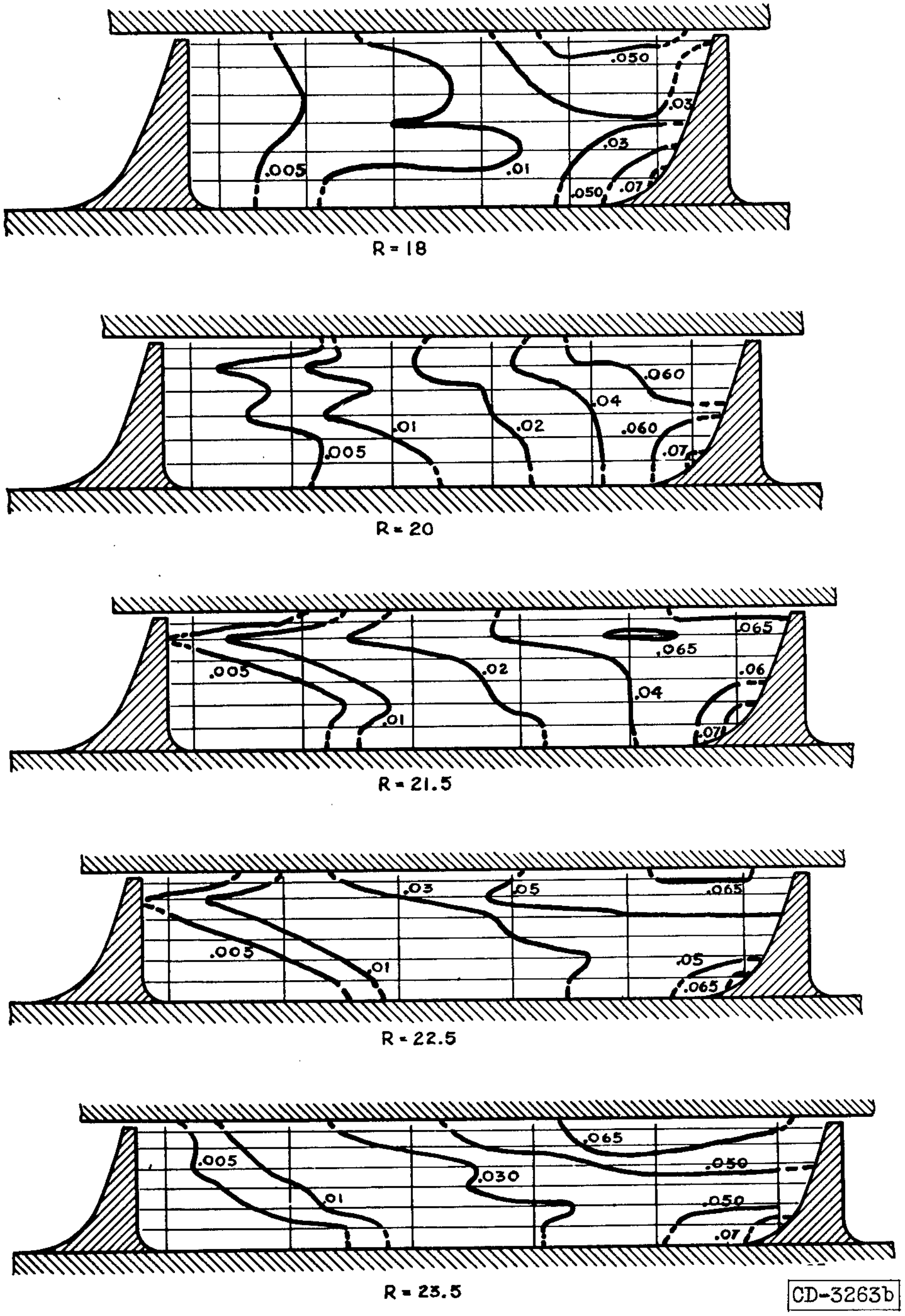

(c) Concluded. Cross-sectional view of total-pressure-loss distribution.

Figure 14. - Concluded. Flow characteristics in rotating passage for six levels between hub and shroud at corrected weight flow of 19.6 pounds per second.

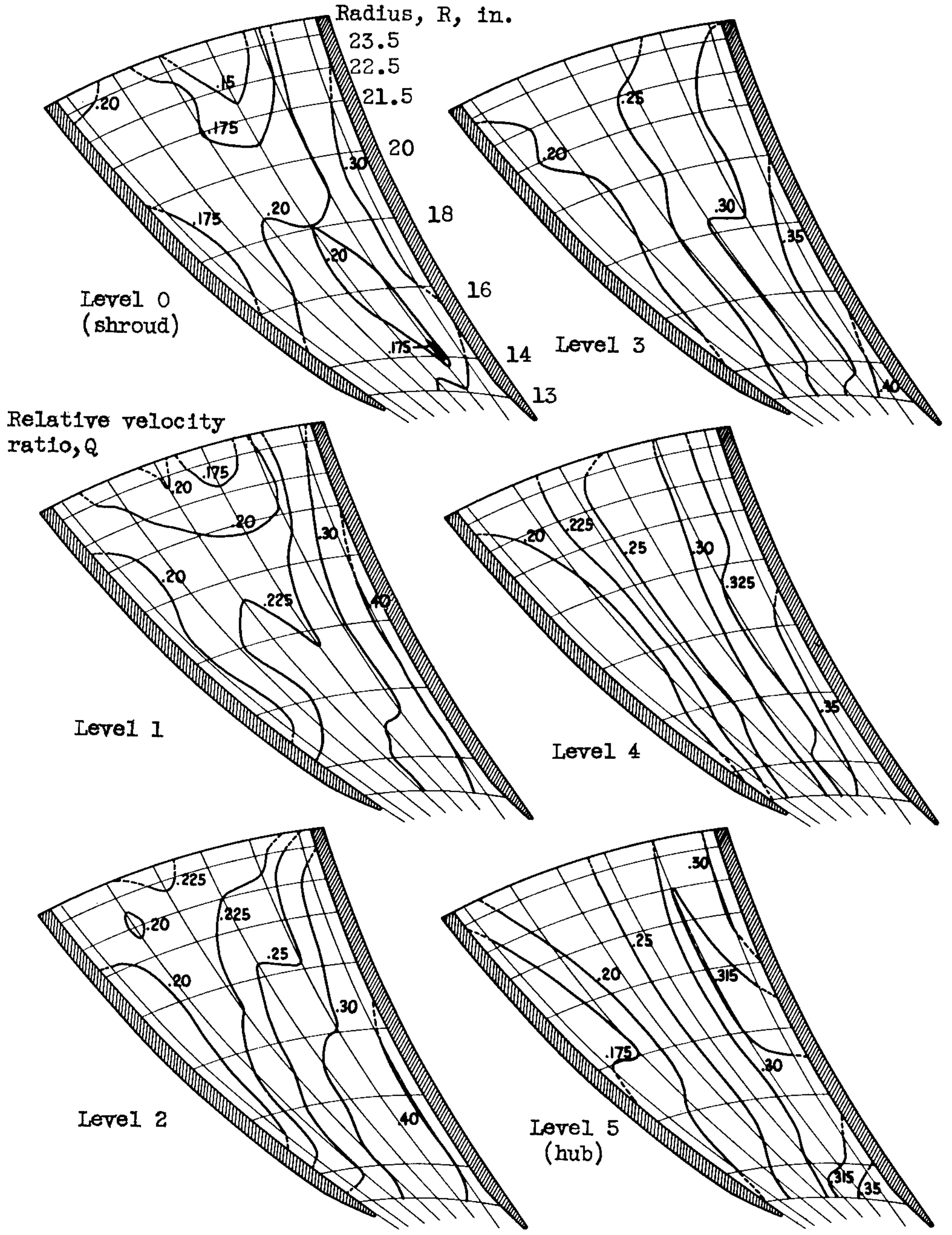

(a) Relative velocity distribution.

Figure 15. - Flow characteristics in rotating passage for six levels between hub and shroud at corrected weight flow of 25.4 pounds per second.

3083

CM-6 back

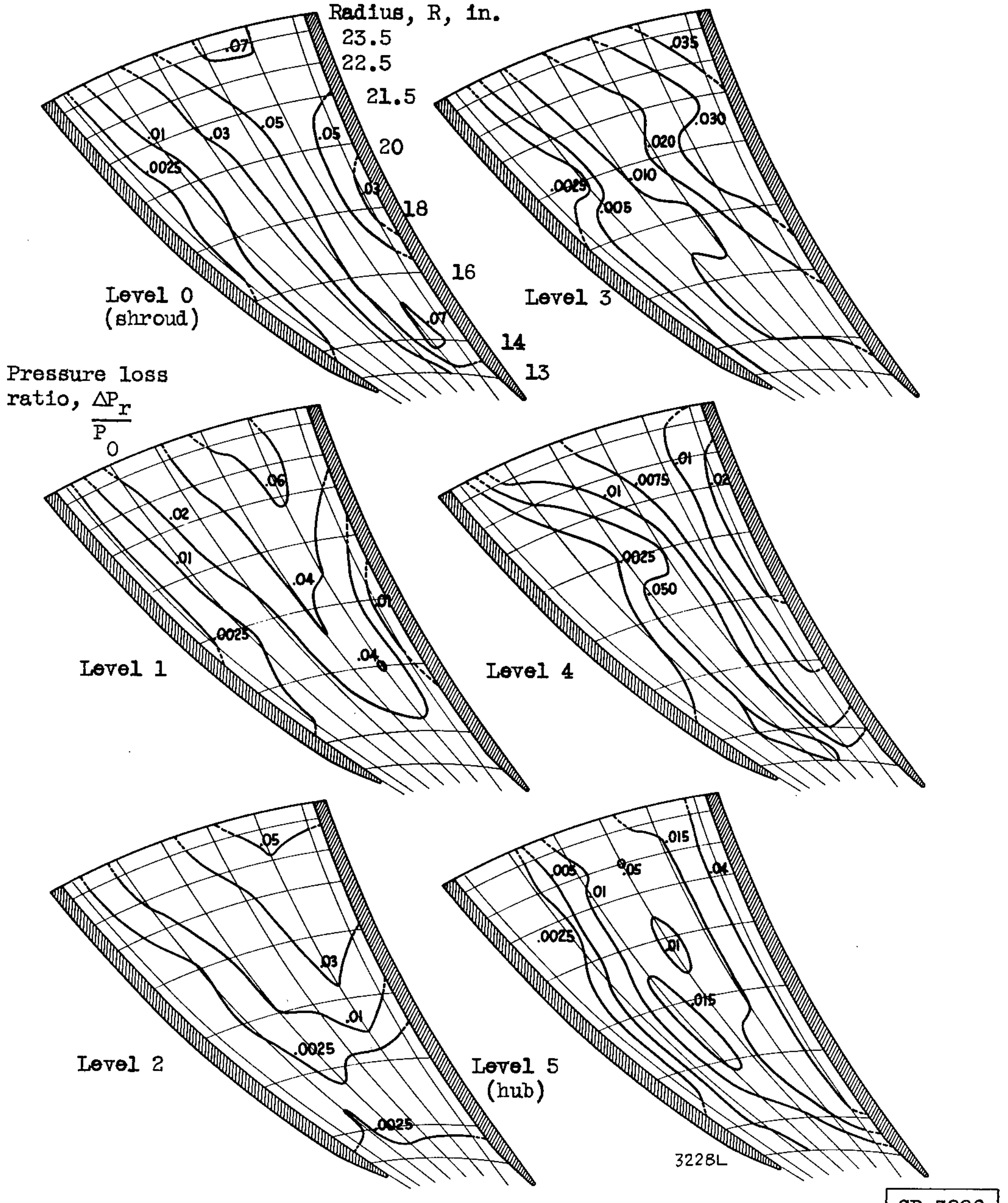

(b) Total-pressure-loss distribution.

Figure 15. - Continued. Flow characteristics in rotating passage for six levels between hub and shroud at corrected weight flow of 25.4 pounds per second.

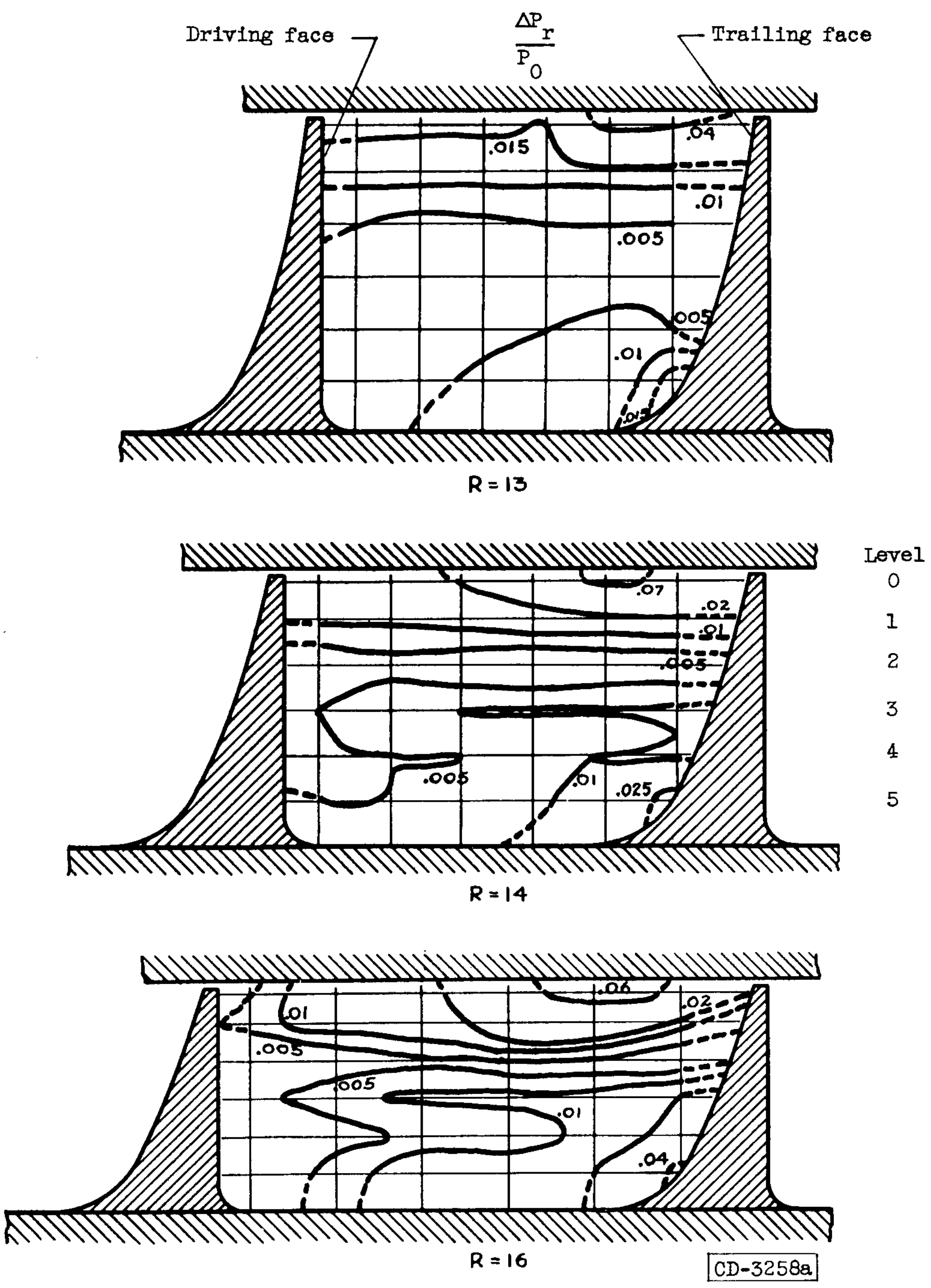

(c) Cross-sectional view of total-pressure-loss distribution.

Figure 15. - Continued. Flow characteristics in rotating passage for six levels between hub and shroud at corrected weight flow of 25.4 pounds per second.

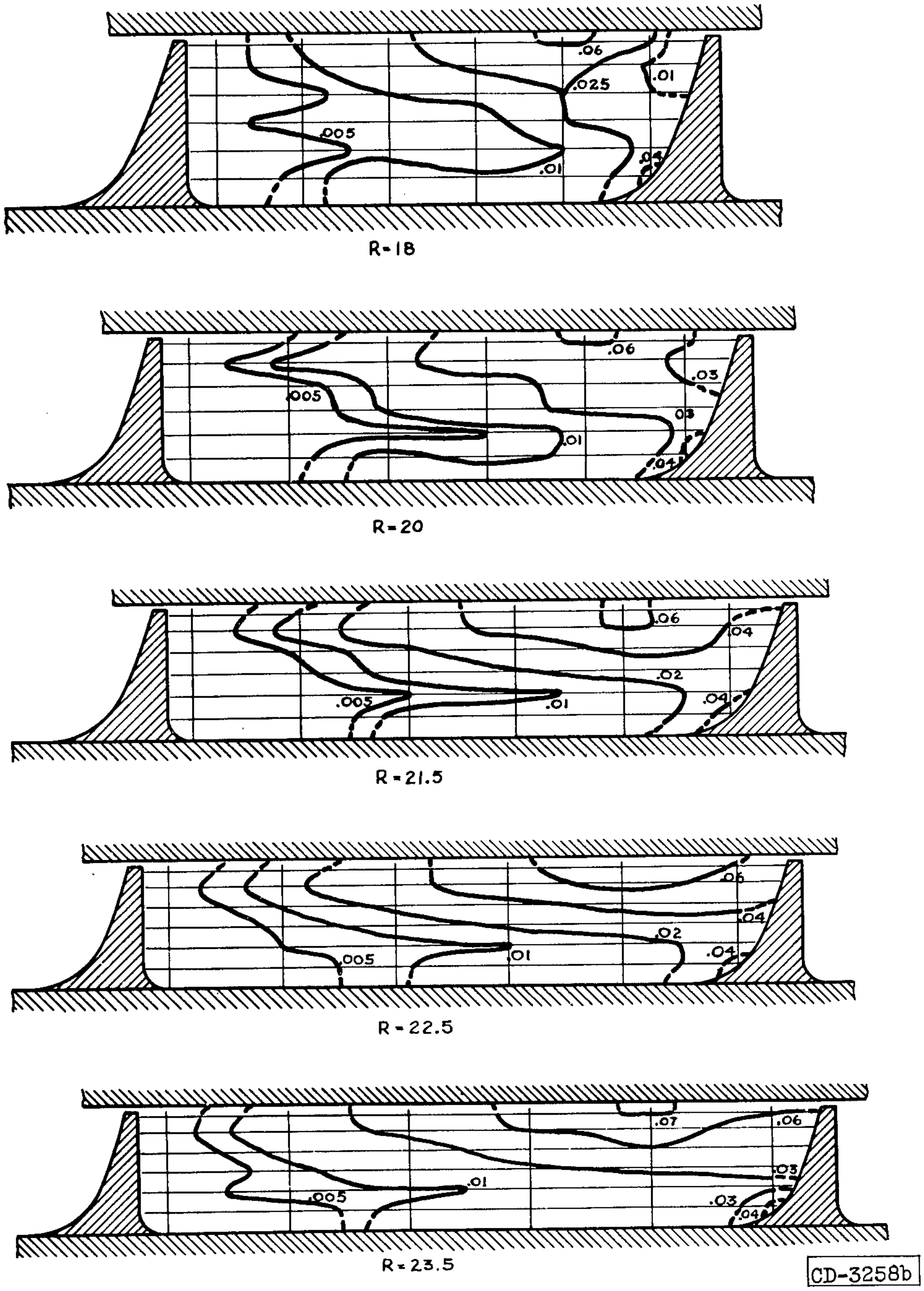

CD-3258b

(c) Concluded. Cross-sectional view of total-pressure-loss distribution.

Figure 15. - Concluded. Flow characteristics in rotating passage for six levels between hub and shroud at corrected weight flow of 25.4 pounds per second.

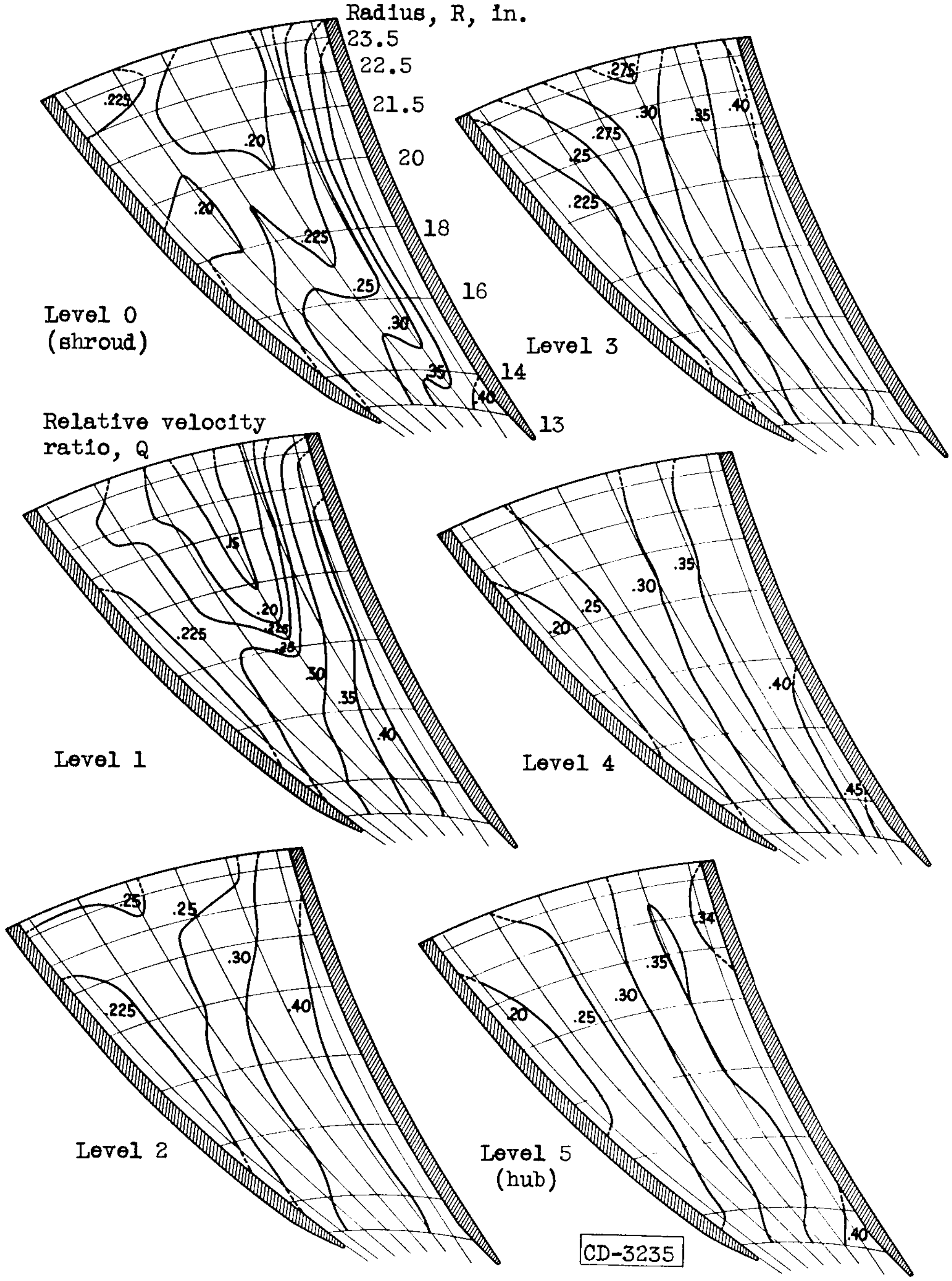

(a) Relative velocity distribution.

Figure 16. - Flow characteristics in rotating passage for six levels between hub and shroud at corrected weight flow of 29.3 pounds per second.

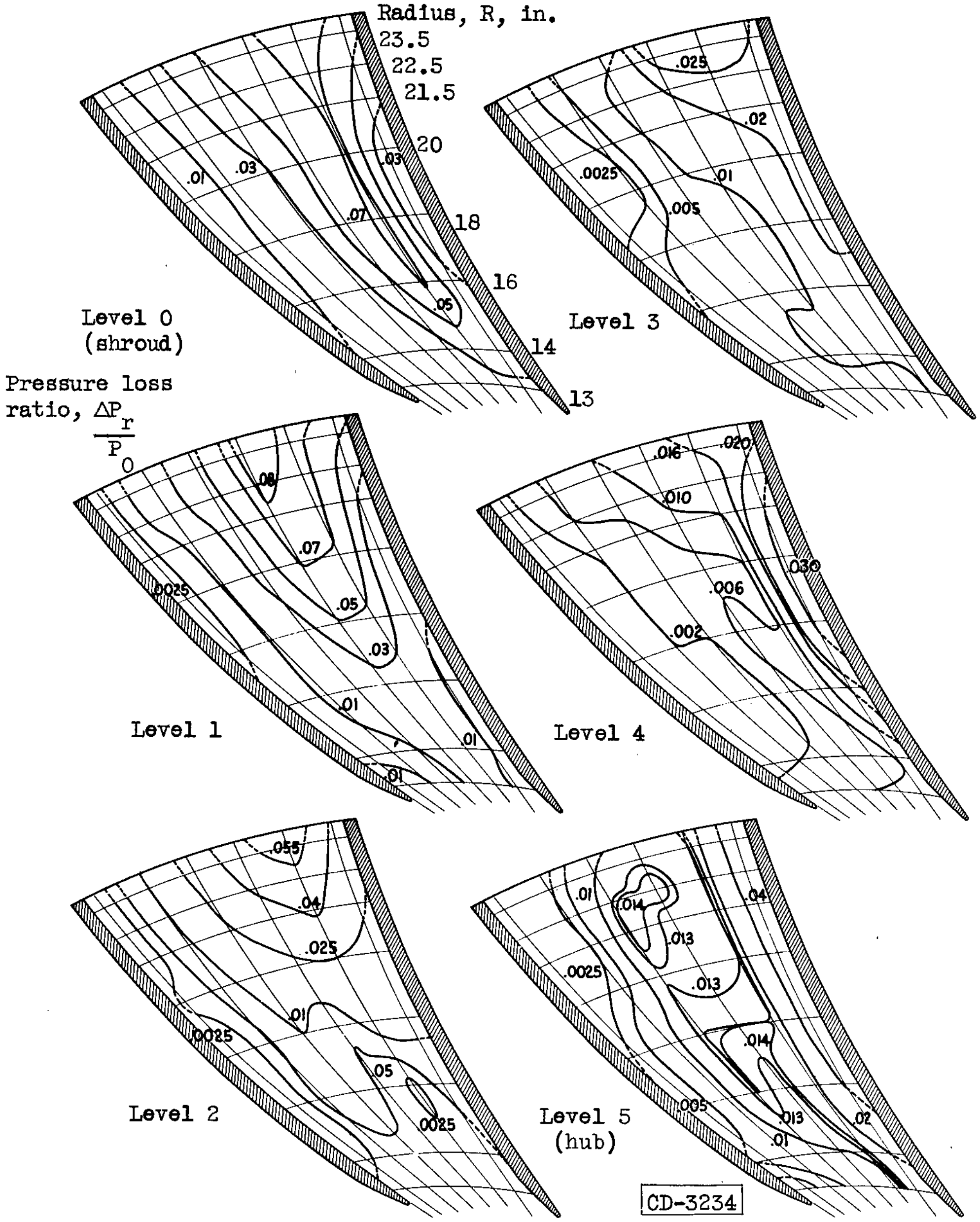

(b) Total-pressure-loss distribution.

Figure 16. - Continued. Flow characteristics in rotating passage for six levels between hub and shroud at corrected weight flow of 29.3 pounds per second.

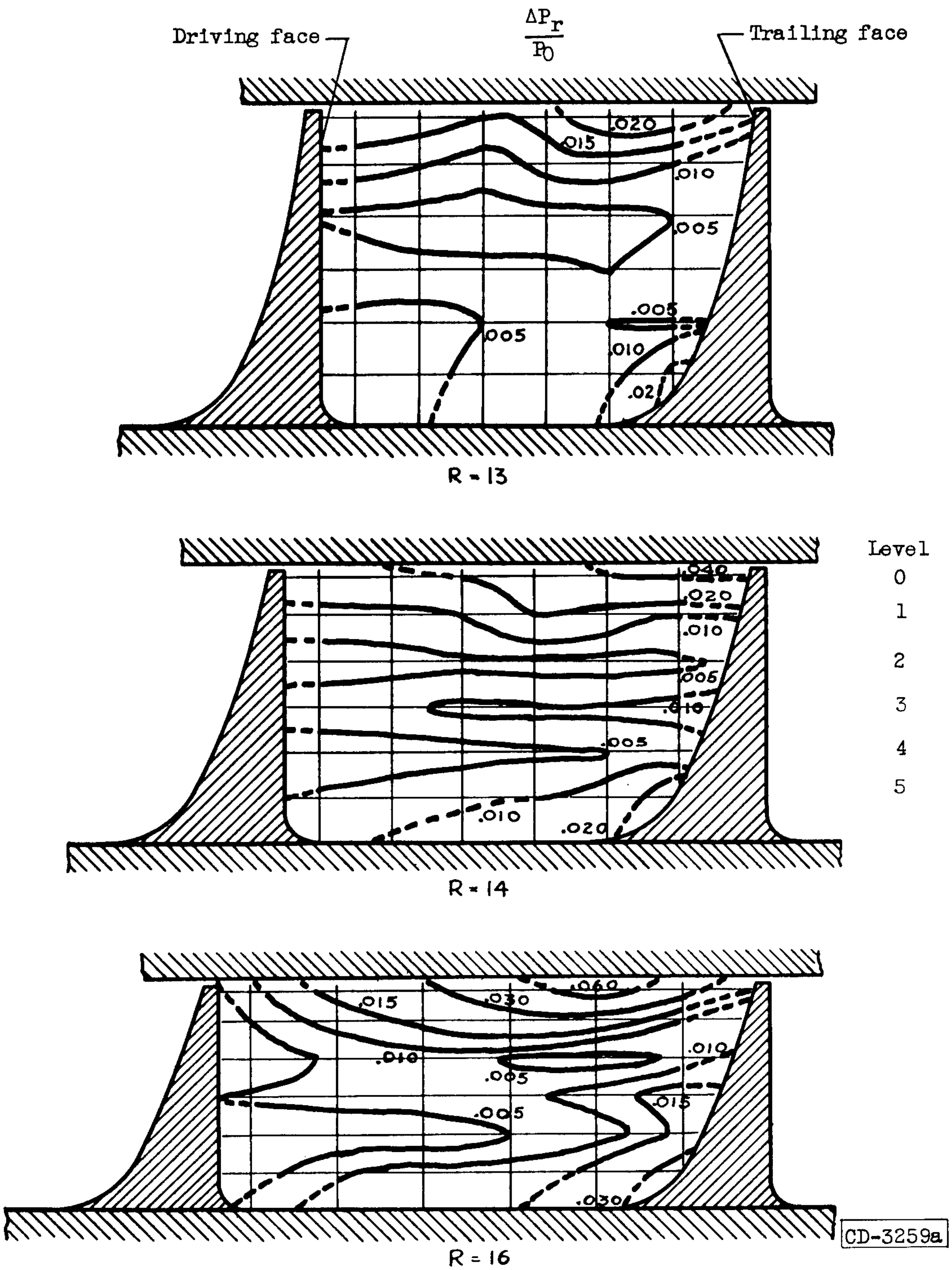

(c) Cross-sectional view of total-pressure-loss distribution.

Figure 16. - Continued. Flow characteristics in rotating passage for six levels between hub and shroud at corrected weight flow of 29.3 pounds per second.

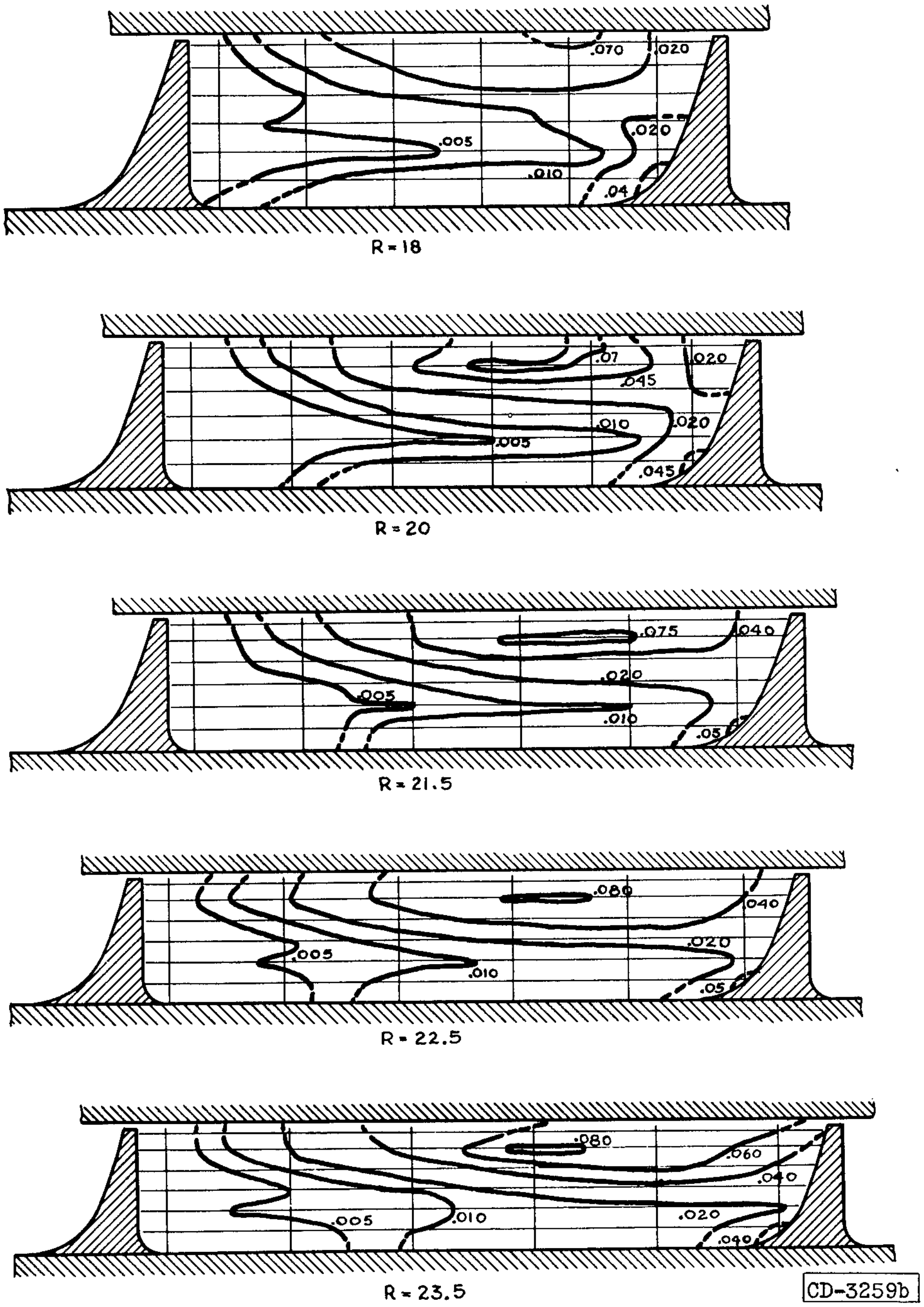

(c) Concluded. Cross-sectional view of total-pressure-loss distribution.

Figure 16. - Concluded. Flow characteristics in rotating passage for six levels between hub and shroud at corrected weight flow of 29.3 pounds per second.

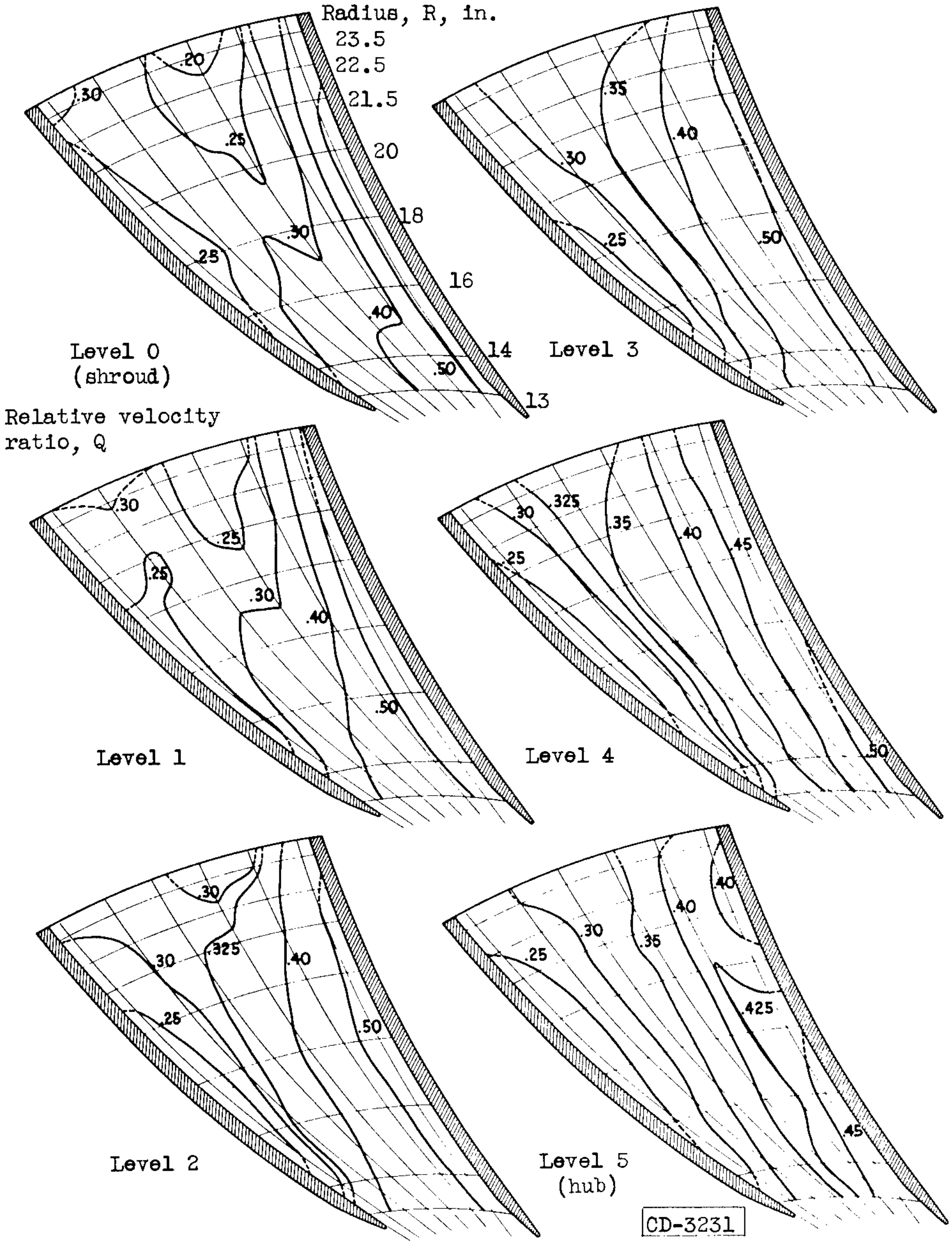

(a) Relative velocity distribution.

Figure 17. - Flow characteristics in rotating passage for six levels between hub and shroud at corrected weight flow of 36.2 pounds per second.

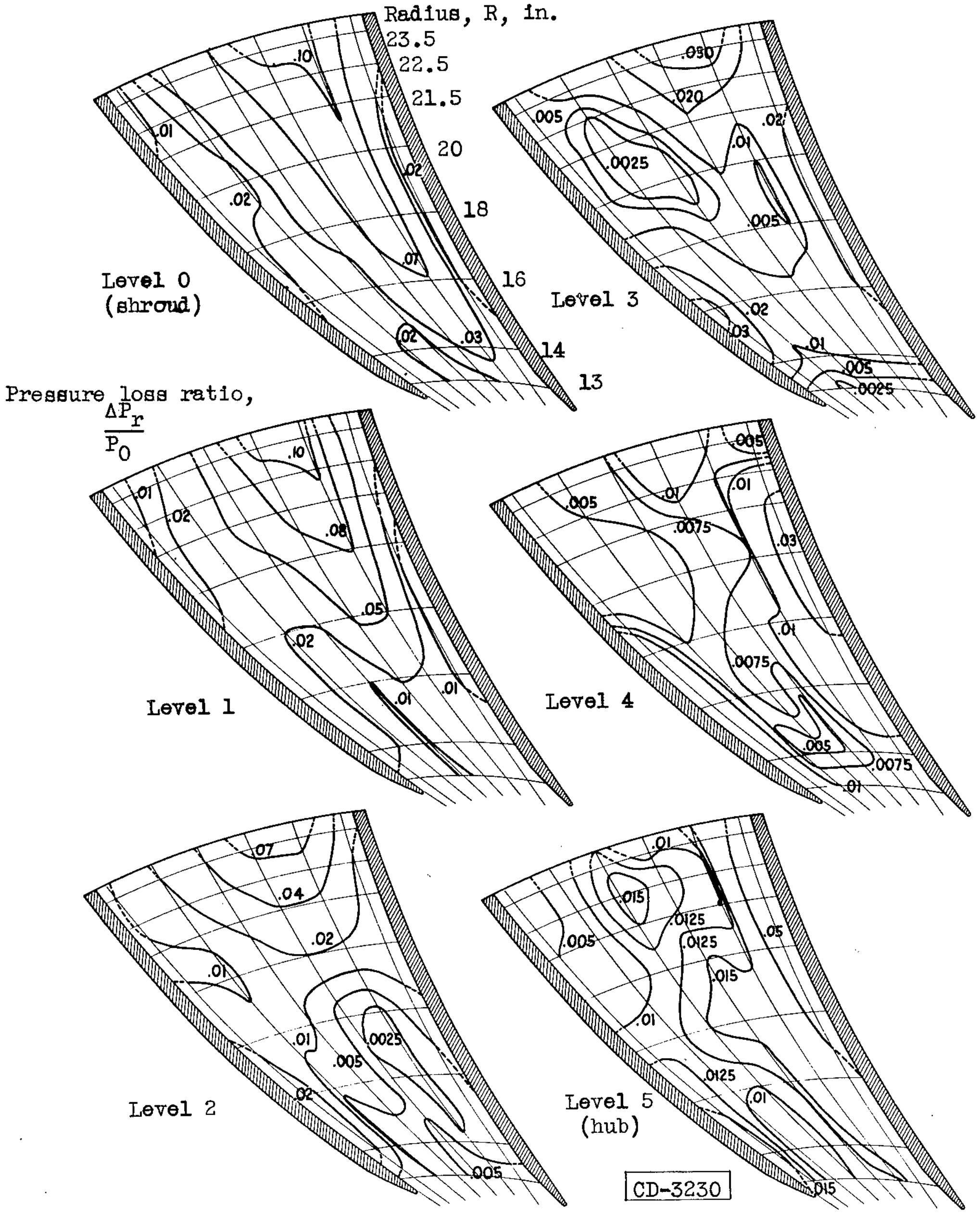

(b) Total-pressure-loss distribution.

Figure 17. - Continued. Flow characteristics in rotating passage for six levels between hub and shroud at corrected weight flow of 36.2 pounds per second.

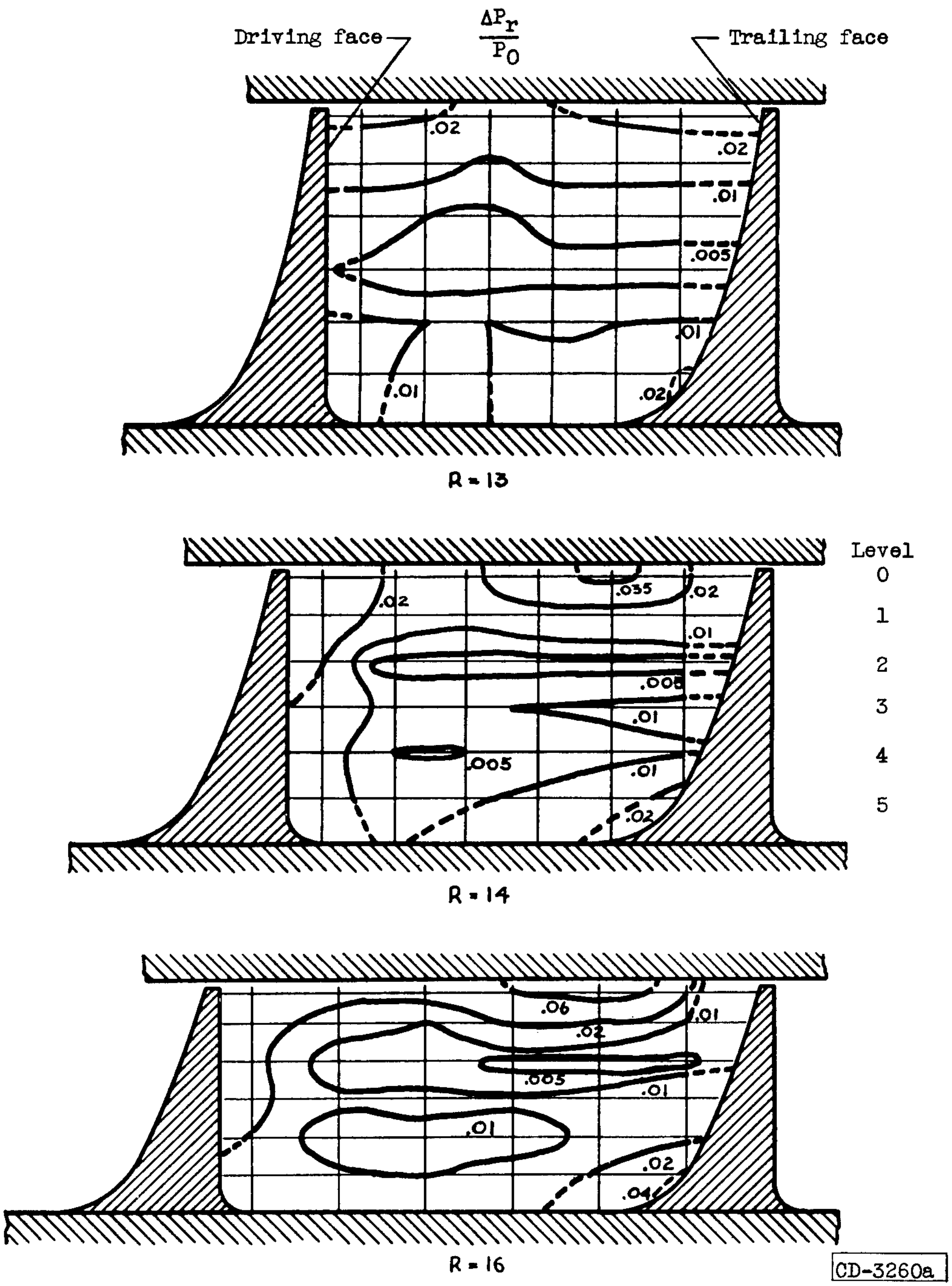

CD-3260a

(c) Cross-sectional view of total-pressure-loss distribution.

Figure 17. - Continued. Flow characteristics in rotating passage for six levels between hub and shroud at corrected weight flow of 36.2 pounds per second.

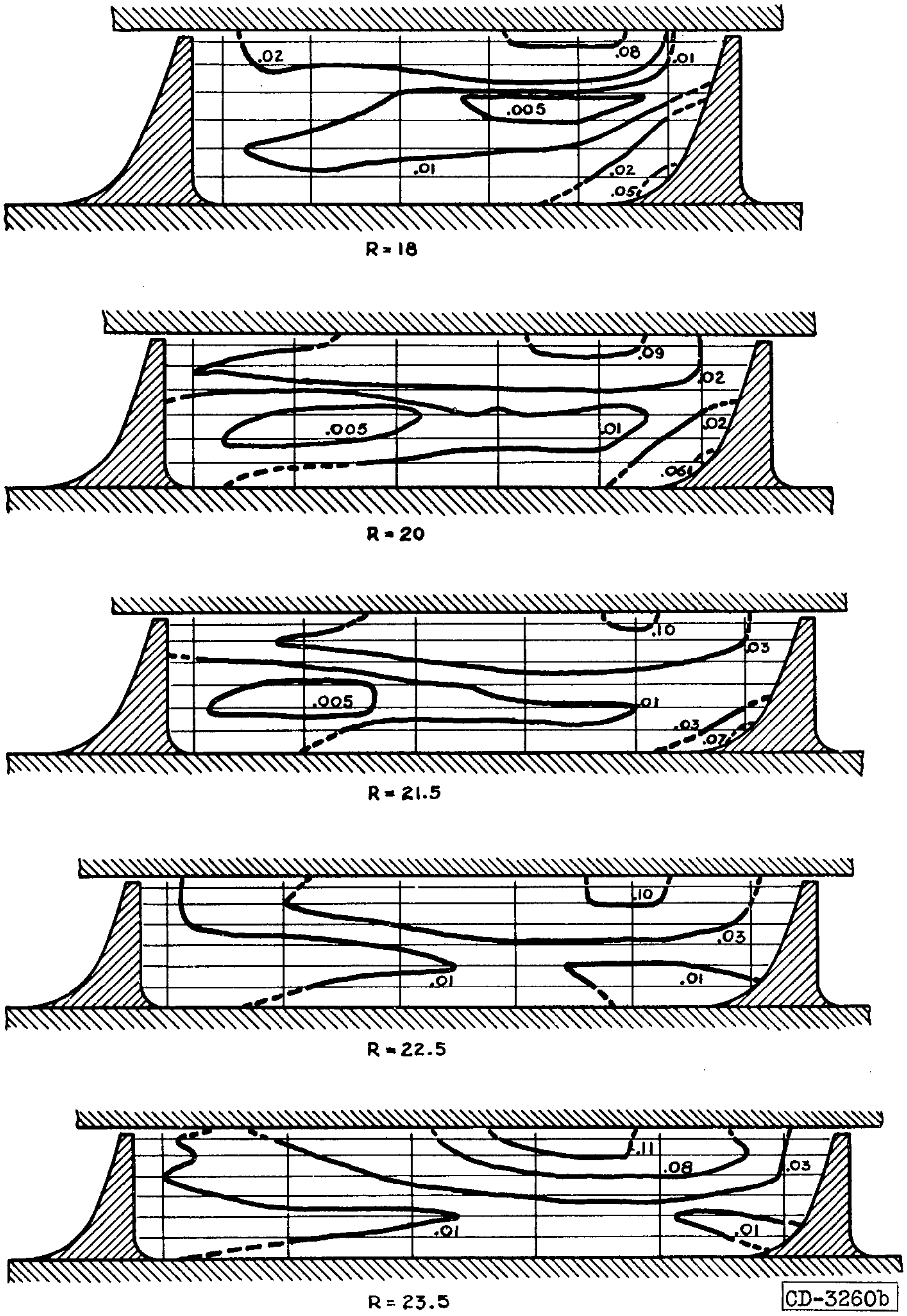

(c) Concluded. Cross-sectional view of total-pressure-loss distribution.

Figure 17. - Concluded. Flow characteristics in rotating passage for six levels between hub and shroud at corrected weight flow of 36.2 pounds per second.

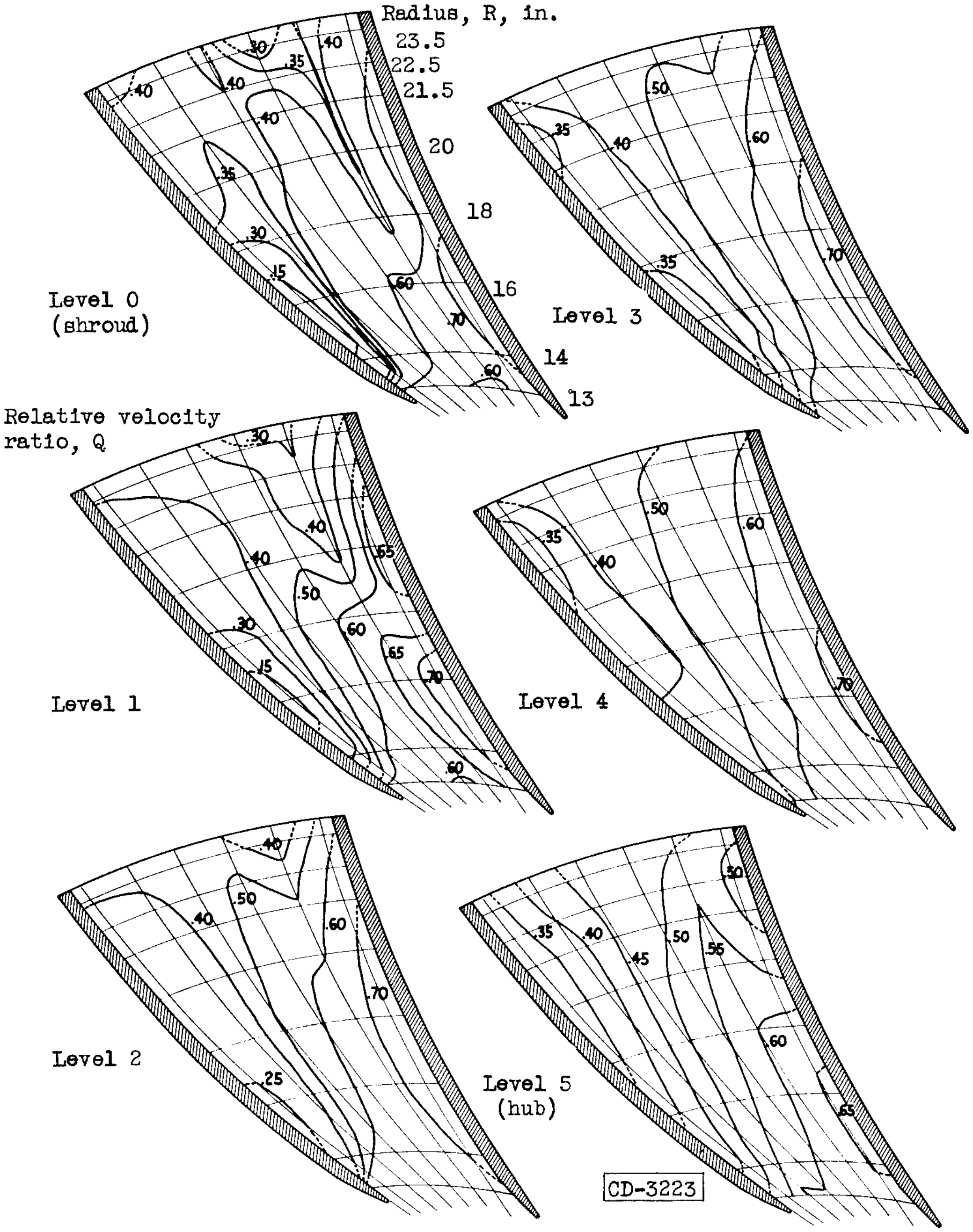

(a) Relative velocity distribution.

Figure 18. - Flow characteristics in rotating passage for six levels between hub and shroud at corrected weight flow of 45.1 pounds per second.

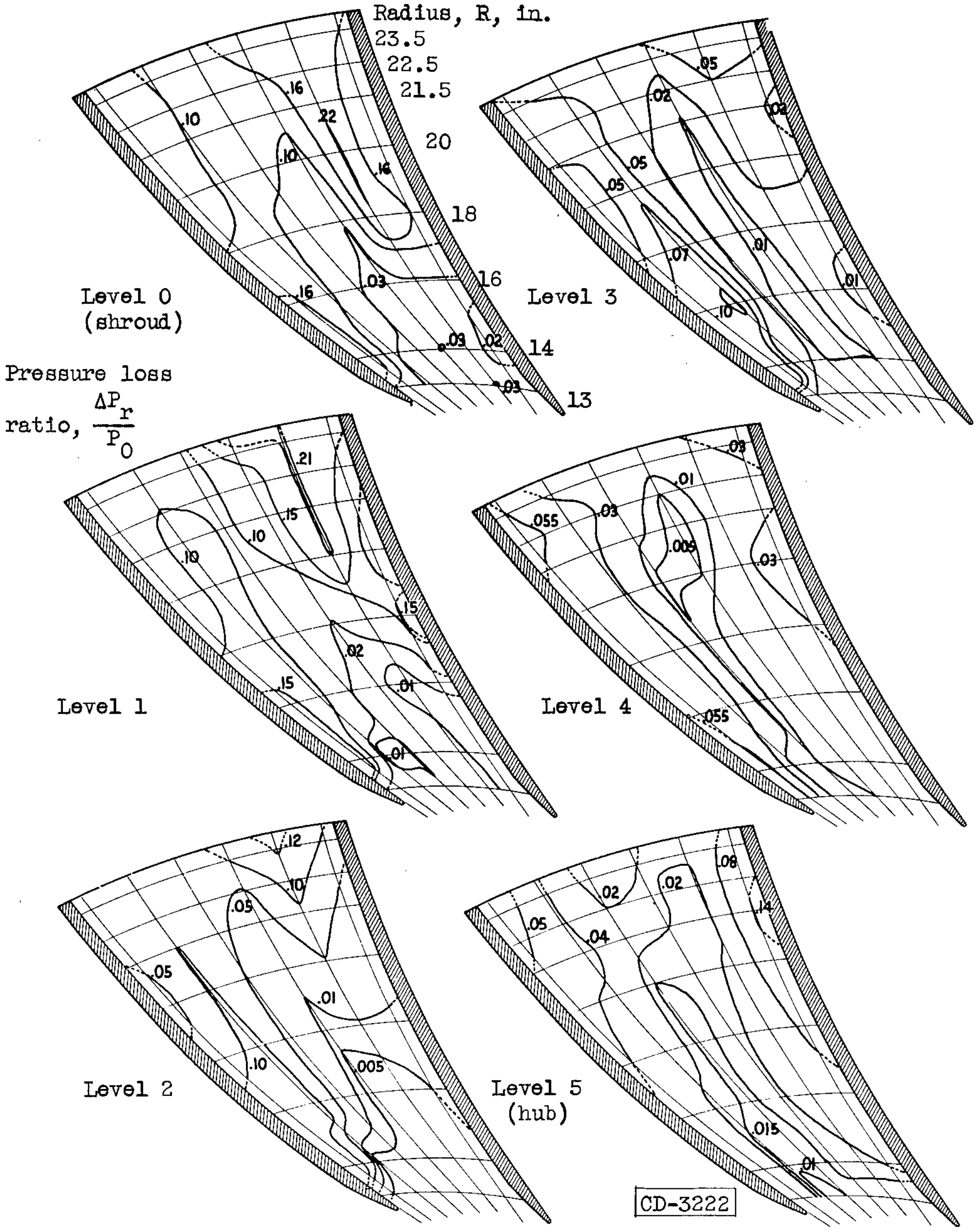

(b) Total-pressure-loss distribution.

Figure 18. - Continued. Flow characteristics in rotating passage for six levels between hub and shroud at corrected weight flow of 45.1 pounds per second.

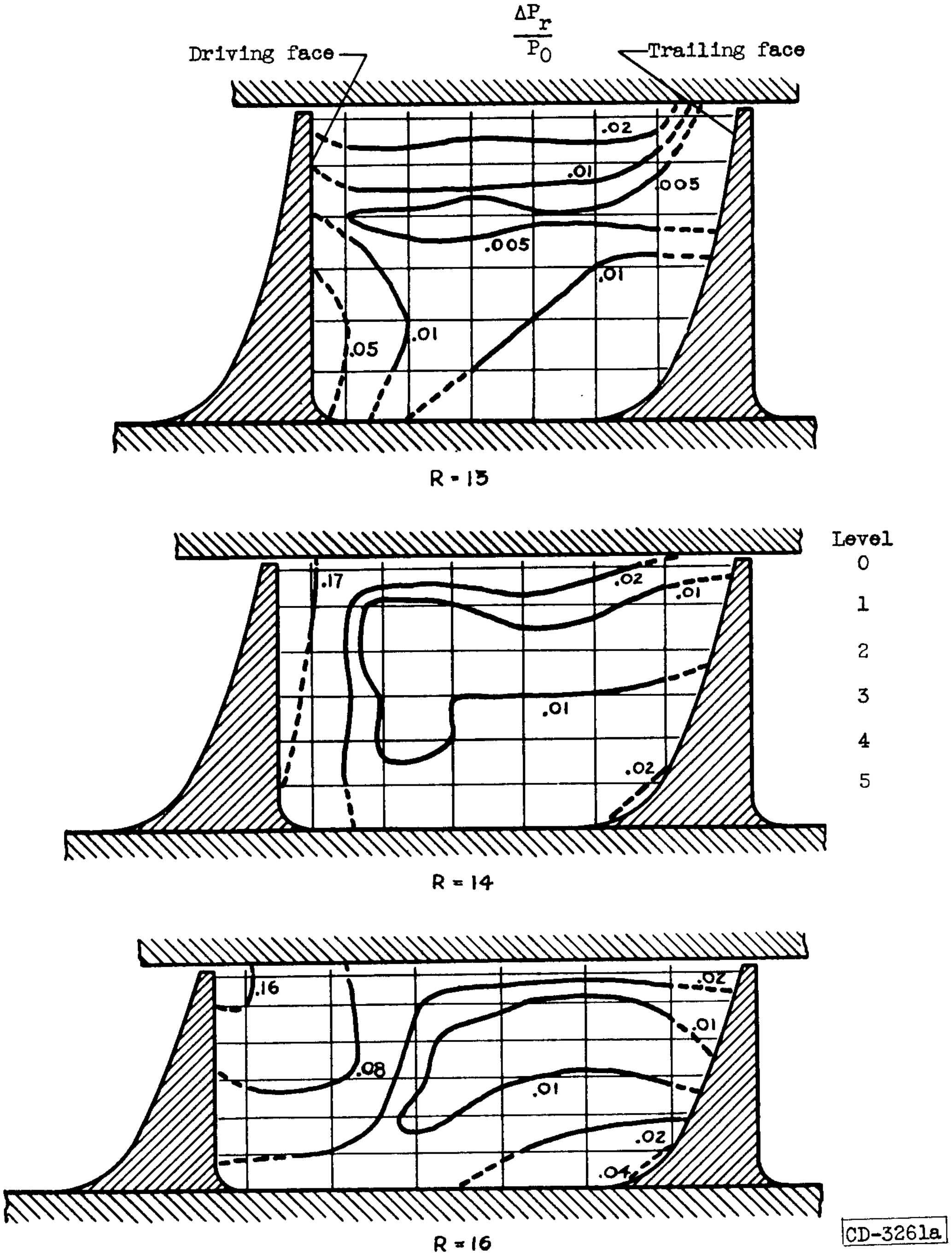

(c) Cross-sectional view of total-pressure-loss distribution.

Figure 18. - Continued. Flow characteristics in rotating passage for six levels between hub and shroud at corrected weight flow of 45.1 pounds per second.

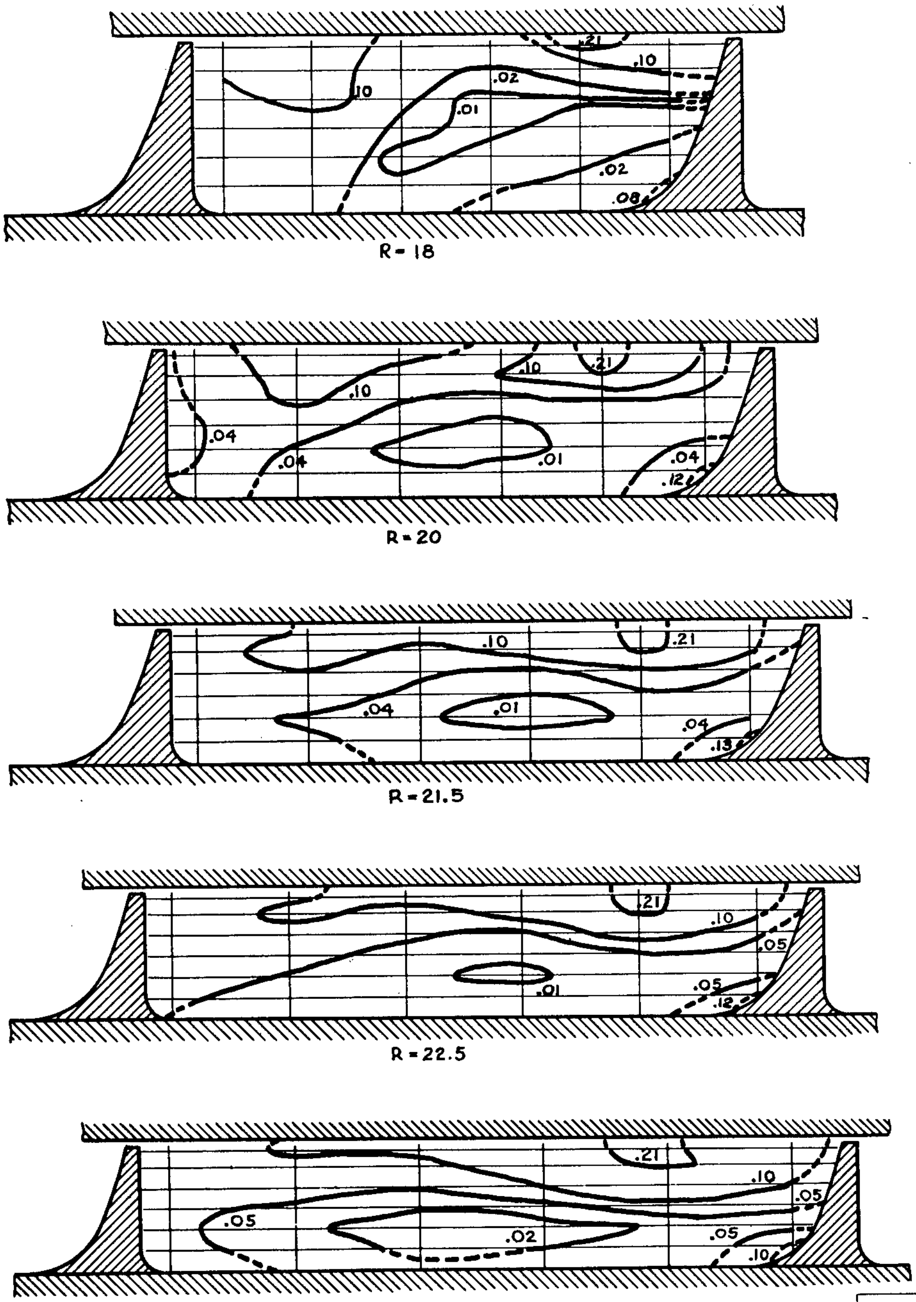

CD-3261b

(c) Concluded. Cross-sectional view of total-pressure-loss distribution.

Figure 18. - Concluded. Flow characteristics in rotating passage for six levels between hub and shroud at corrected weight flow of 45.1 pounds per second.

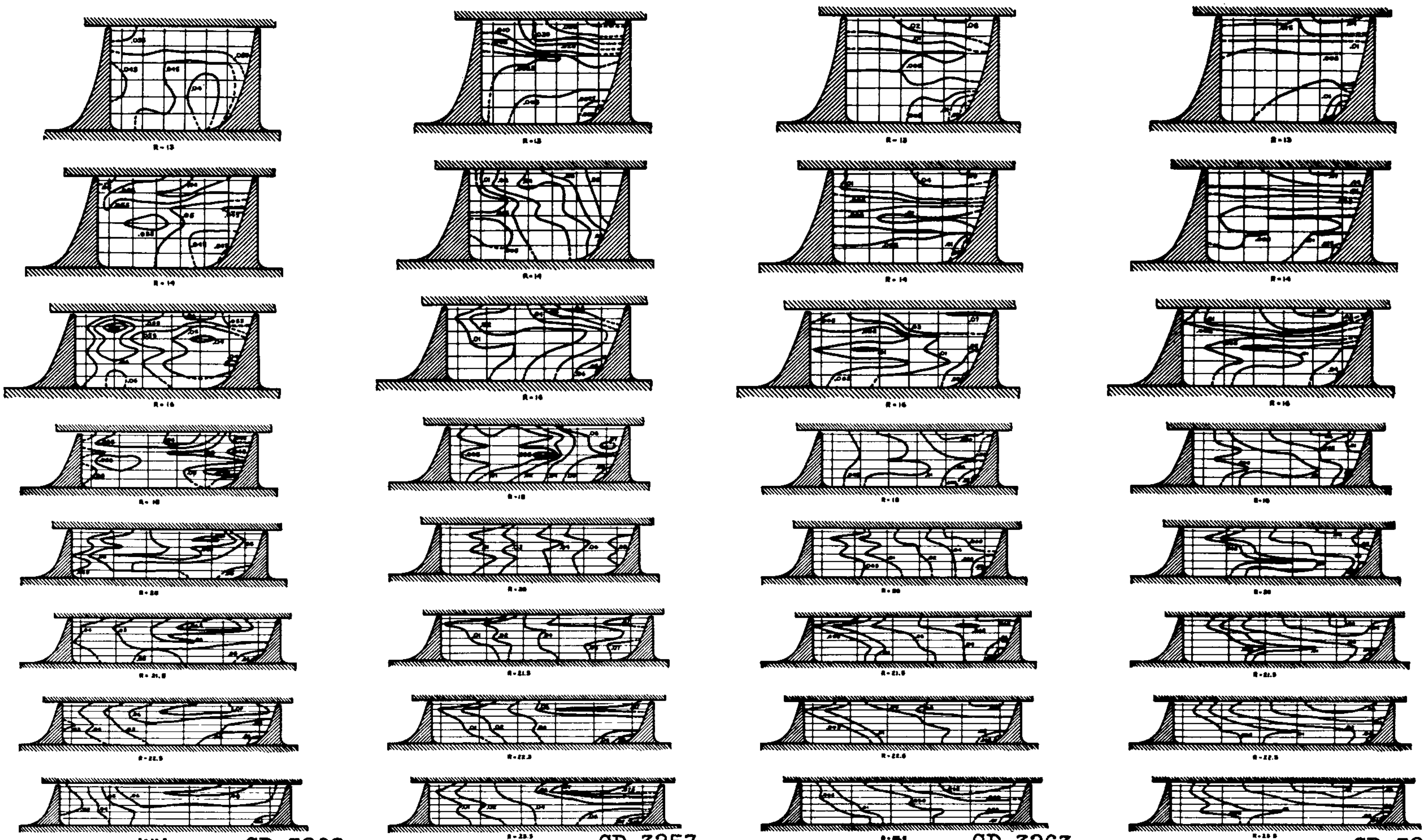

CD-3262 $\frac{W\sqrt{\theta}}{\delta} = 11.2$

CD-3257 $\frac{W\sqrt{\theta}}{\delta} = 15.6$

CD-3263 $\frac{W\sqrt{\theta}}{\delta} = 19.6$

CD-3258 $\frac{W\sqrt{\theta}}{\delta} = 25.4$

Figure 19. - Comparison of all passage cross-sectional views of total-pressure-loss distribution.

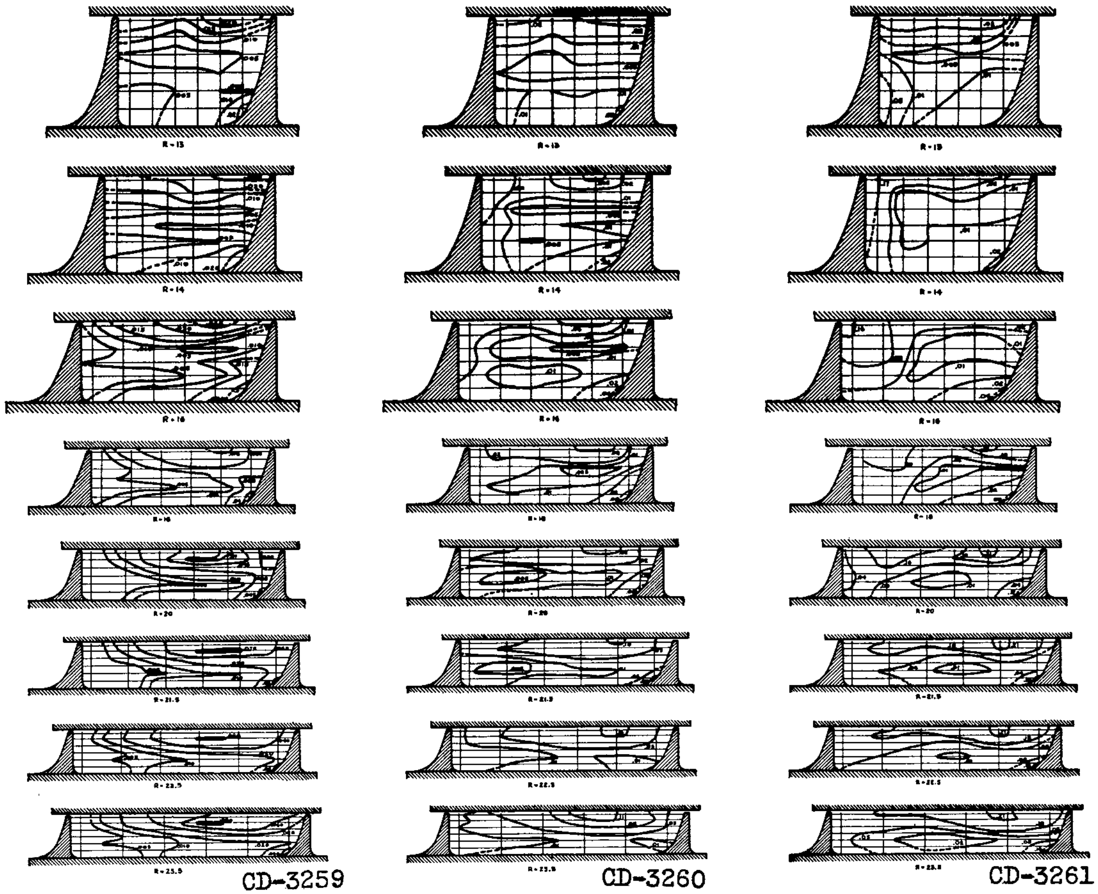

CD-3259

$\frac{W\sqrt{\theta}}{\delta} = 29.3$

CD-3260

$\frac{W\sqrt{\theta}}{\delta} = 36.2$

CD-3261

$\frac{W\sqrt{\theta}}{\delta} = 45.1$

Figure 19. - Concluded. Comparison of all passage cross-sectional views of total-pressure-loss distribution.

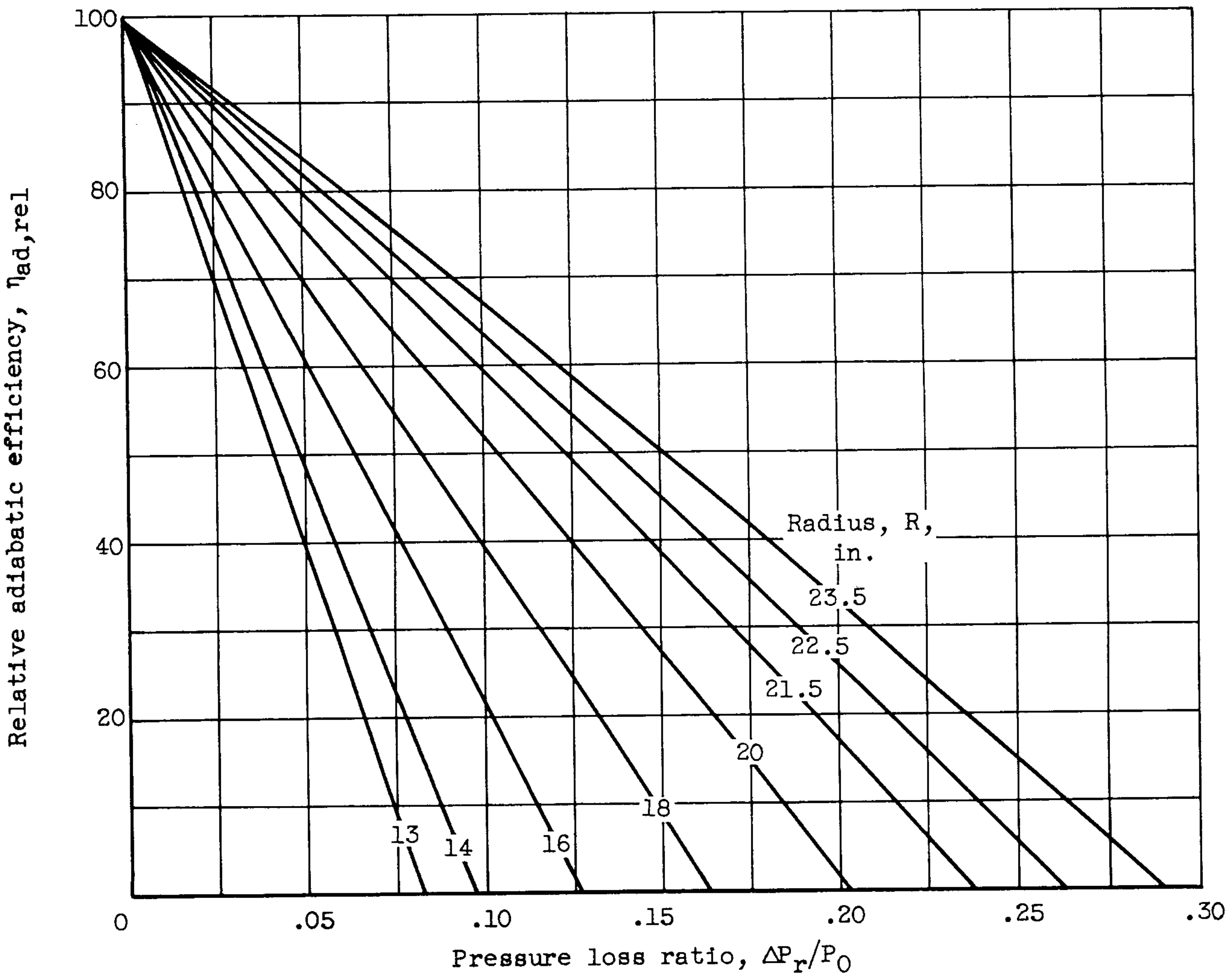

Figure 20. - Variation in relative adiabatic efficiency with pressure loss ratio at given impeller radii.

3083

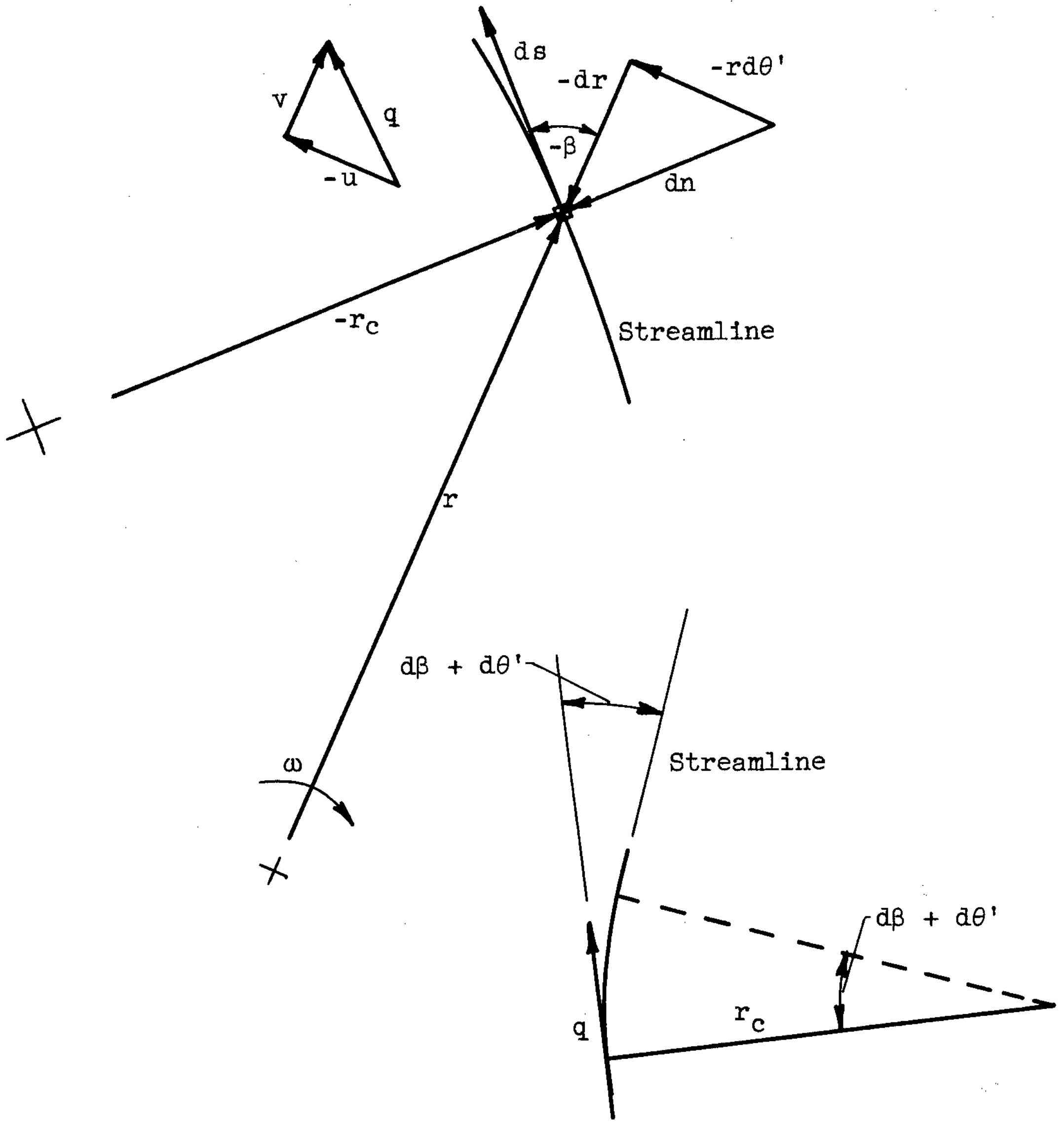

Figure 21. - Orientation of quantities used in obtaining equation (7).

3083

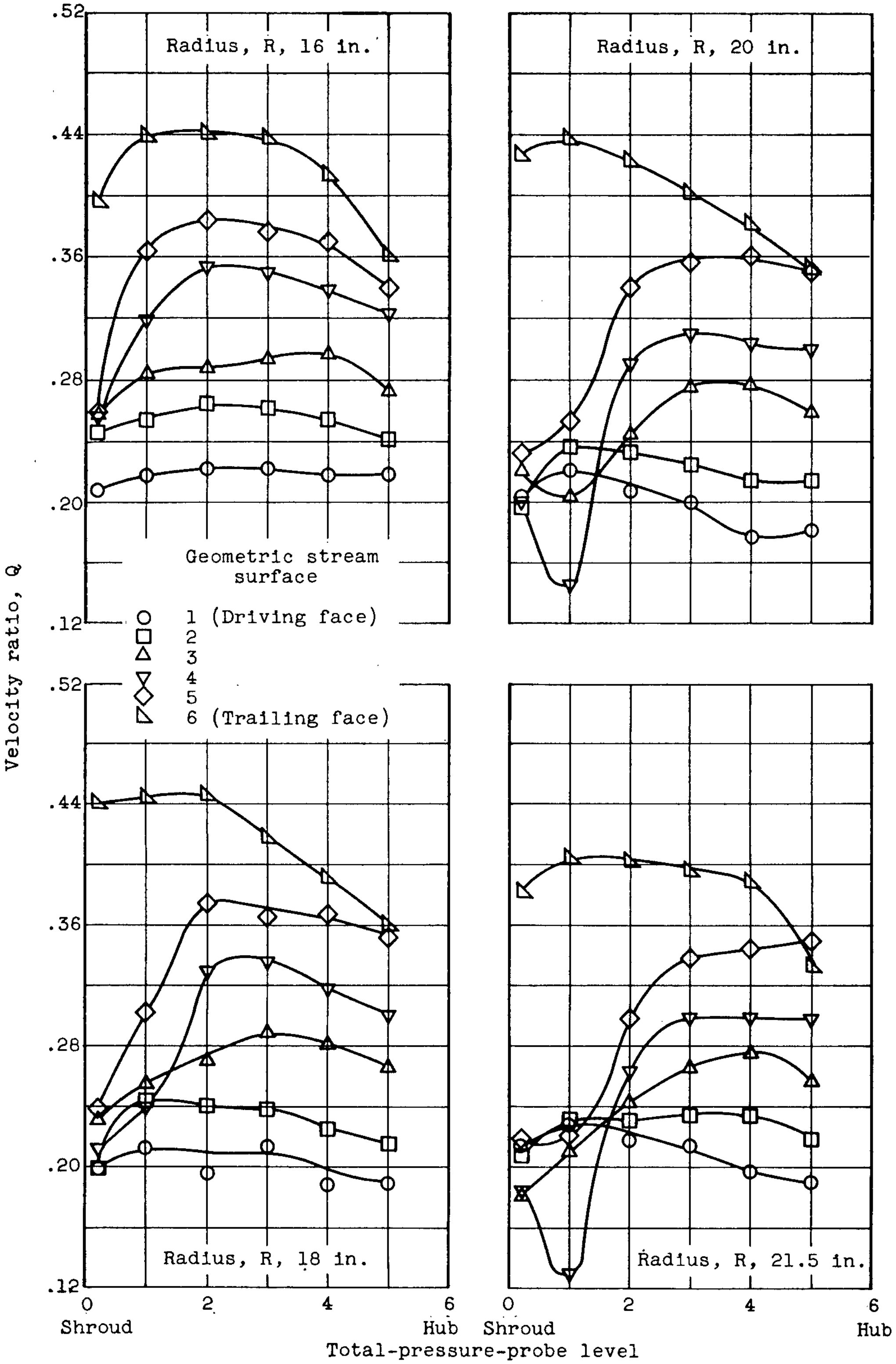

Figure 22. - Shroud-to-hub velocity profiles across geometric stream surfaces at four radii for corrected weight flow of 29.3 pounds per second.

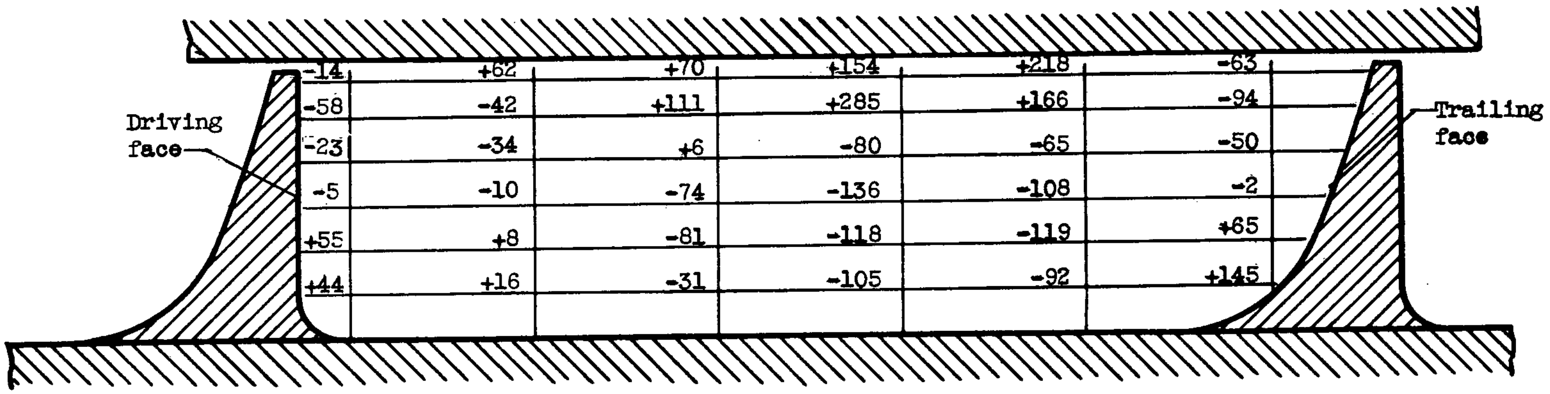

(a) Accelerative pressure gradients based on actual velocities and assumption that flow is directed along geometric streamlines (plus sign indicates acceleration toward trailing face).

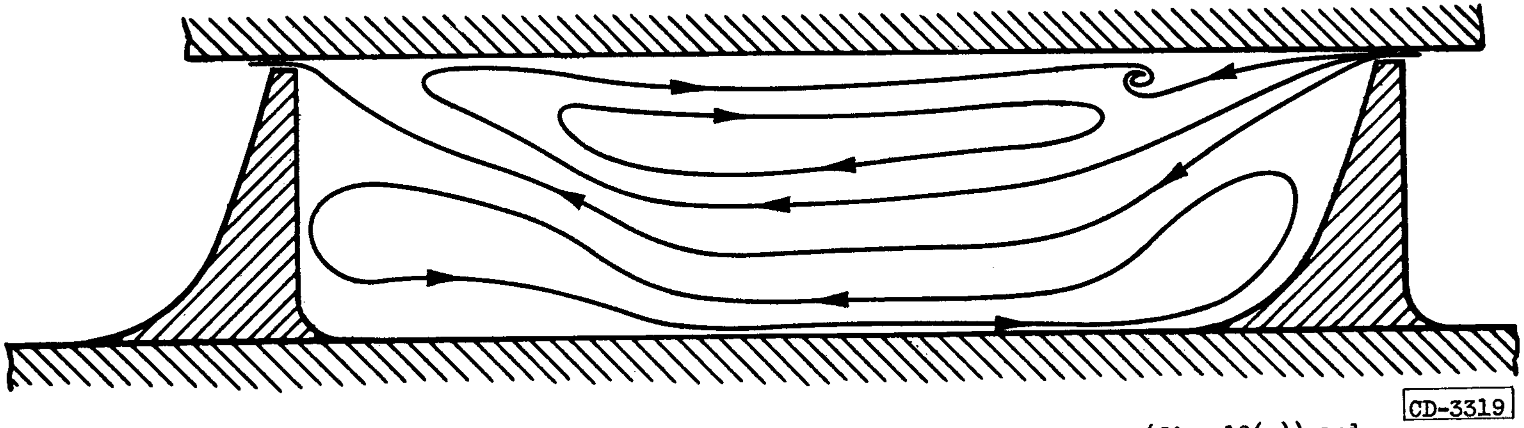

(b) Possible directions of secondary flow based on pressure loss contours (fig. 16(c)) and accelerative pressure gradients.

Figure 23. - **Secondary** flow at 20-**inch** radius at **weight** flow of 29.3 **pounds per second.**

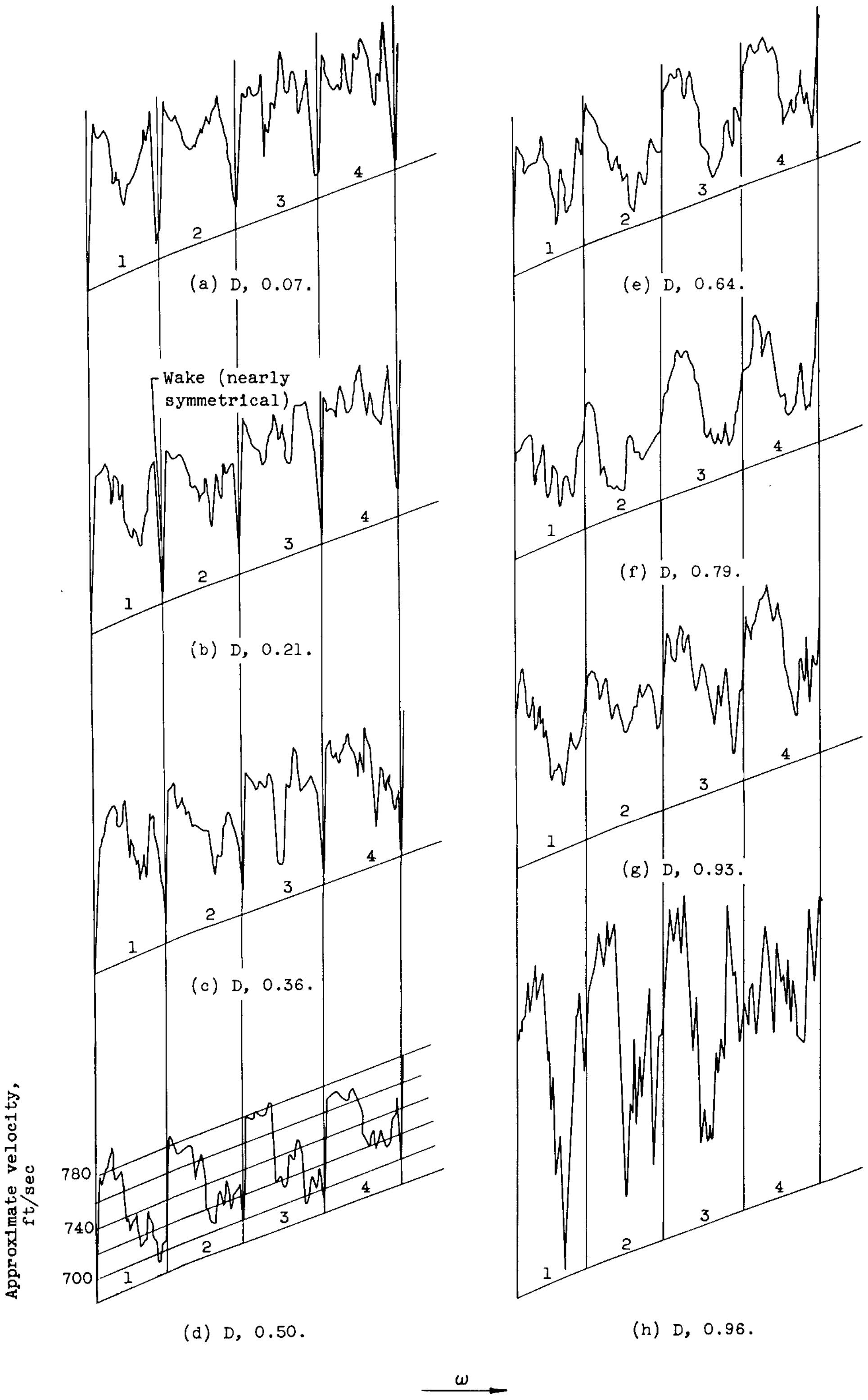

(a) D, 0.07.

(b) D, 0.21.

(c) D, 0.36.

(d) D, 0.50.

(e) D, 0.64.

(f) D, 0.79.

(g) D, 0.93.

(h) D, 0.96.

Figure 24. - Hub-to-shroud survey with velocity variation across blade passage at exit (four passages). Equivalent weight flow, 26 pounds per second. Driving-to-trailing face across passage is in direction of rotation ω. (Numbers refer to successive passages.) (From ref. 8.)

NACA-Langley - 2-12-54 - 1000

NACA TN 3101
National Advisory Committee for Aeronautics.
STUDY OF THREE-DIMENSIONAL INTERNAL FLOW DISTRIBUTION BASED ON MEASUREMENTS IN A 48-INCH RADIAL-INLET CENTRIFUGAL IMPELLER. Joseph T. Hamrick, John Mizisin and Donald J. Michel. February 1954. 64p. diagrs., photos. (NACA TN 3101)

A study of the loss and velocity distribution in a radial flow impeller was made. It is indicated that secondary flows within the boundary layer and leakage through the blade-to-shroud clearance space result in a concentration of low-energy air at approximately 80 percent of the passage width from the pressure face at the shroud. Comparison of the data from internal measurements made for the impeller of this investigation with hot-wire anemometer studies made at the outlet of a similar impeller indicates that much can be learned about the internal flow picture with hot-wire surveys alone.

Copies obtainable from NACA, Washington

1. Flow, Compressible (1. 1. 2)
2. Internal Aerodynamics (1. 4)
3. Compressors - Radial Flow (3. 6. 1. 2)

I. Hamrick, Joseph T.
II. Mizisin, John
III. Michel, Donald J.
IV. NACA TN 3101